Universidade do Minho
Escola de Engenharia

João António Mesquita Barbosa

Development of an X-ray detection system based on polymer-based scintillator composites

Dezembro de 2016

Development of an X-ray detection system based on polymer-based scintillator composites
João António Mesquita Barbosa
UMinho | 2016

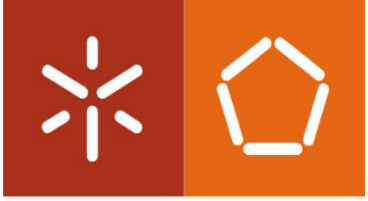

Universidade do Minho
Escola de Engenharia

João António Mesquita Barbosa

Development of an X-ray detection system based on polymer-based scintillator composites

Dissertação de Mestrado

Mestrado em Engenharia Eletrónica Industrial e de Computadores

Trabalho efetuado sob a orientação de:

Professor Doutor Senentxu Lanceros-Mendez

Professor Doutor José Gerardo Vieira Rocha

Doutor Hélder Filipe Alves de Castro

Dezembro de 2016

ACKNOWLEDGMENTS

In the first place, I want to thank my supervisors, Professor Gerardo Rocha and Professor Senentxu Lanceros-Mendez for their readiness and for pointing me in the right direction during this last year, helping to overcome the problems faced in the realization of this master's thesis.

Grateful thanks to Professor Vítor Correia for his help and guidance, and to Juliana Oliveira for her tireless and constant support and patience during all the stages of this work. Thanks also to all the Electroactive Smart Materials Group colleagues for the support and constant good mood in the lab. Thanks to Mr. Azevedo from DCT for all availability and assistance during the experimental tests.

My warmest and special thanks to my family, specially to my parents, brother, grandparents and cousin, for all encouragement and support because none of this would be possible without you.
Special thanks to all my friends and co-adventurers for all that I've learned and grown with you and ours experiences.

Thanks to all my professors and the DEI staff, for their instructions and support during the course. Also, I want to give my thankfulness to everybody who interacted and helped me during my periods abroad, especially to the people in BCMaterials in Bilbao and the professors of University of Zielona Góra

I am most grateful to Tuna Universitária do Minho for welcoming and integrating me in this family and friendship, which made me grow a lot, both personally and professionally. Thanks to ARCUM and all its elements for the conviviality and friendship during these years.

Finally, I want to specially thank all my course colleagues and partners in these years. Thank you for all support, help, fellowship, motivations, sleepless nights and learning. Especially thanks to Xeixas, Chuck, Cabo, Pires, Gui, Pdr, Poisson, Xee, Smile, Rua, Mini, Virgílio, Bé, Rapha and Nobre. This work, like me, has a bit of all you!

ABSTRACT

Nowadays, radiation processing techniques are used in many fields and are undergoing fast developments. The demand for improving spatial resolution and to obtain more clear and accurate images, while reducing the radiation doses, have led to the replacement of the traditional techniques based on X-ray films processing by digital processing techniques, that combine high efficiency electronic sensors with computing algorithms. However, these current techniques and radiation detection methods face severe limitations and high costs when large areas or flexible applications are involved.

In this work an X-ray detection system was developed, with the aim of presenting an innovative solution, efficient, flexible, and capable of being produced in a large area and at a low cost. To achieve these objectives, a Styrene-Ethylene/Butadiene-Styrene (SEBS) polymer films were prepared, containing scintillator nanoparticles, $Gd_2O_3:Eu^{3+}$, that are responsible for converting X-rays into visible light. These materials present unique characteristics like flexibility, stretchability and easy and low cost production.

It was also developed a compact electronic circuit responsible for acquiring and processing the visible light produced by the scintillator material. This circuit is based on a photodetector matrix and auxiliary components that have to obtain visible light values, multiplex the matrix sensors and communicate the results to a microcontroller.

Thereafter, a firmware to the microcontroller was implemented to control the whole system, from sensors acquisition to sending the data through serial communication to a user interface. The results are displayed and presented to the user in a clear and organized way, allowing the user to make an easy and direct analysis.

Finally, the system was subject to tests according to a previously defined experimental methodology. In these experiments, the system revealed a fluid, solid and clean performance with room for optimization, improvements and adaptation to new and innovative applications.

RESUMO

Actualmente, as técnicas de processamento de radiação são usadas em muitas áreas de investigação e aplicação, ao mesmo tempo que sofrem uma constante e rápida evolução. A necessidade de melhorar a resolução e obter imagens mais claras e precisas, ao mesmo tempo que é reduzida a quantidade de radiação, levaram a que as técnicas tradicionais baseadas no processamento de películas radiográficas fossem sendo substituídas por técnicas de processamento digital, que aliam sensores electrónicos de alta eficiência com programação algorítmica. No entanto, estas técnicas e métodos de detecção de radiação actuais enfrentam duras limitações e elevados custos quando é pretendida a produção de grandes áreas de detecção ou a integração em aplicações flexíveis.

Nesta dissertação é desenvolvido um sistema de detecção de raio-X com o objectivo de apresentar uma solução inovadora, que seja eficiente, flexível e capaz de ser produzida em grandes áreas e a baixo custo. Para cumprir estes objectivos, foi preparada uma matriz polimérica de *Styrene-Ethylene/Butadiene-Styrene* (SEBS) contendo concentrações de nanopartículas cintiladoras, $Gd_2O_3:Eu^{3+}$, responsáveis por converter os raios-X em luz visível. Este material cintilador apresenta características ímpares, como flexibilidade, extensibilidade, baixo custo e fácil produção e replicação.

Foi também desenvolvido um circuito electrónico de reduzidas dimensões, responsável por adquirir e processar a luz visível produzida pelo cintilador. Este circuito foi implementado com base numa matriz de fotodetectores e componentes electrónicos auxiliares que têm como função obter os valores de luz visível, efectuar a multiplexagem dos sensores da matriz, e enviar os dados para o microcontrolador.

Posteriormente foi desenvolvido um *firmware* para o microcontrolador capaz de efectuar o controlo de todo o sistema, desde a aquisição dos sensores até ao envio dos dados através de comunicação série para uma interface com o utilizador. Os resultados são apresentados ao utilizador de uma forma clara e organizada, permitindo uma análise directa e facilitada destes.

Por fim, o sistema foi sujeito a testes de acordo com uma metodologia previamente definida. Nestes testes, o sistema revelou um desempenho fluído, sólido e direto, havendo espaço para a sua optimização, melhoramento e adaptação para novas aplicações.

INDEX

LIST OF FIGURES

LIST OF TABLES

List of Abbreviations and Acronyms

APS	Active Pixel Sensor
CCD	Charge Coupled Device
CMOS	Complementary Metal Oxide Semiconductor
COM	Communication Channel
DOD	Drop-On-Demand
IC	Integrated Circuit
INH	Inhibit Channel
LCTF	Liquid Crystal Tunable Filters
LED	Light-emission Diode
LSB	Least-significant Bit
MCU	Microcontroller Unit
MSB	Most-significant Bit
MUX	Multiplexer
OLED	Organic Light-emission Diode
PCB	Printed Circuit Board
POPOP	(1,4-bis (2-(5-phenioxazolil))-benzol
PPO	2,5-dipheniloxazol
PPS	Passive Pixel Sensor
PS	Polystyrene
PVA	Poly(Vinyl Alcohol)
PVDF	Poly(vinylidene Fluoride)
SBS	Styrene-Butadiene-Styrene
SEBS	Styrene-Ethylene/Butadiene-Styrene
SPI	Serial Peripheral Interface
TPE	Thermoplastic Elastomers
TTL	Transistor-Transistor Logic
TWI	Two Wire Interface

1. INTRODUCTION

In this chapter an introduction to the subject addressed in this master's thesis is made, presenting the motivations and the objectives proposed for this work, while its organization and structure are described and discussed.

1.1 Objectives and Motivation

The aim of radiology is to improve the resolution of its techniques in order to obtain more clear and precise images and results while reducing the emitted radiation dose [1]. This radiation decrease presents some benefits, reducing its possible harmful effects as well as its power consumption. Consequently, the traditional techniques based on X-ray films processing are being overtaken and substituted by digital processing techniques that combine the use of high efficiency electronic sensors with algorithmic programming [1].

Radiation detectors can be produced by following two distinct approaches: direct and indirect method [2]. The direct method uses photoconductive materials with high X-ray absorption capability but that require a high bias voltage to operate. The indirect method uses scintillators, materials that absorb X-rays and convert its energy into visible light [3]. However, both methods still face severe limitations and high costs when large areas or flexible applications are involved.

Polymer composites based on scintillator nanoparticles that convert radiation into visible light allow to design and implement large and flexible detection areas as well as innovative applications since they present high efficiency, flexibility and low cost production [4, 5].

This work focuses on the development of a system capable of converting X-rays by using polymer composites based on scintillator nanoparticles, as well as detecting the visible light through photodetectors. The system developed will allow not only to absorb and convert the radiation, but to measure and acquire the visible light resulting from the conversion, and clearly and correctly display the results obtained.

In a future work it will be possible to use the developed composites and the elaborated photodetection principles in the implementation of a printed circuit-based system, notably using printed photodetection matrices. This implementation will allow the integration and flexibility of the whole system as well as the production of large detection areas without limitations and at a low cost.

1.2 Thesis Structure

Chapter 1: In this chapter, the master's thesis subject is introduced, presenting the motivation and objectives proposed while its structure and organization are described and discussed.

Chapter 2: This chapter focuses on a review of the state of art about the work's subject. Firstly, one reviews the radiology background and evolution, along with the different detection methods. The focus of the matter then shifts to different scintillators and radiation detectors types. Finally, the photodetection techniques are reviewed.

Chapter 3: This chapter presents the preparation of the scintillator to be used in the system as well as the materials to be prepared to develop the polymer composites based on scintillator nanoparticles. It is also presented a brief review of the technologies used to develop printed circuits.

Chapter 4: Throughout this chapter one describes the detection system design and assembly as well as the implementation of the microcontroller firmware and its main functions.

Chapter 5: This chapter explains the methodology adopted in the experimental tests, presenting and analysing the results obtained from them.

Chapter 6: In this chapter a final conclusion is presented, based on what was developed and analysed throughout this work. Some corrections, improvements and new approaches are also suggested, as they should be taken into account in future research.

2. STATE OF ART

This chapter focuses on a review of the state of art about the work's subject. Firstly, one reviews the radiology background and evolution, along with the different detection methods. The focus of the matter then shifts to different scintillators and radiation detectors types. Finally, the photodetection techniques are reviewed.

2.1 The Evolution of Radiography

2.1.1 X-Rays Discover and Conventional Radiography

German physicist Wilhem Conrad Röentgen (Figure 1) discovered a new type of radiation on November 8th, 1895, while working with a Crooke tube, used to investigate the cathode rays [6-8].

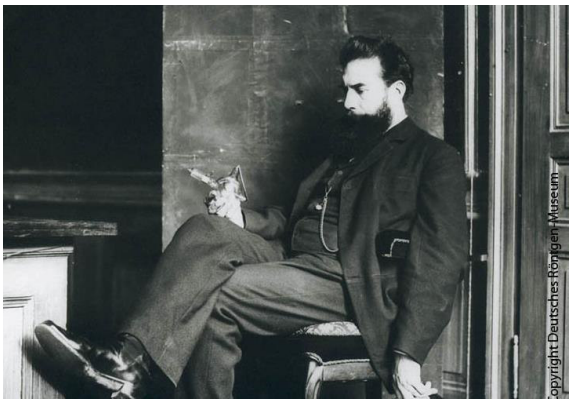

Figure 1. German physicist Wilhem Conrad Röentgen [9]

Later, on December 22nd, 1895, Röentgen made the first X-ray photograph using his wife's hand. In this photograph it is possible to distinguish her hand bones and a metal ring (Figure 2) [9].

Figure 2. X-ray Photograph of Anna Bertha Röentgen's hand [9]

The X-rays are a kind of electromagnetic radiation that have a wavelength in the range of 0.01 to 10 nanometres (nm), corresponding to frequencies between 30 petahertz to 30 exahertz ($3x10^{16}$ Hz to $3x10^{19}$ Hz), being these wavelengths typically shorter than those of UV rays and longer than those of gamma rays (Figure 3) [10].

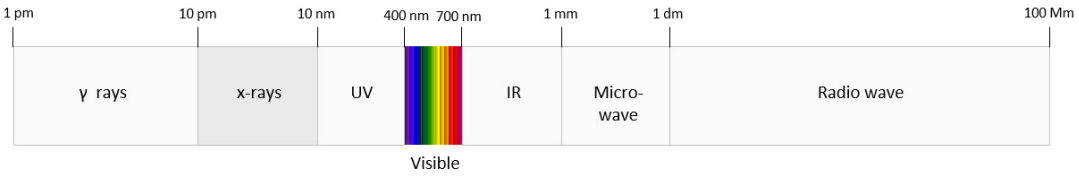

Figure 3. Electromagnetic spectrum [10]

This discovery led to a revolution in many fields, mainly in Medicine, as it grants us the possibility of image diagnosis. When penetrating through a body, a beam of X-rays interacts with its atoms. The result is a beam with different patterns of photons which correspond to different types and shapes of tissues and its thickness and constituent elements [11].

Since then, the aim of radiology is to improve the resolution and techniques used in the radiation detection, to obtain more clear and accurate images [1]. However, conventional radiography based on film processing has several and important limitations that must be overcome, such as the high radiation dose required, low quality images, lengthy film processing, and the use of chemicals with high environmental impact [12].

2.1.2 Digital Radiography

The development and application of digital radiology appeared as a result of technology evolution and an alternative to overtake these limitations. Besides eliminating the chemical process [2], this approach presents some advantages, such as [13]:

- Reduction of radiation dose

  In conventional radiography, the radiation dose is determined by the receptors' sensitivity and the film's depth brightness. In digital radiography the only concern involving the radiation dose is due to the relationship signal-noise, that can maintain satisfactory values while reducing the radiation dose. Any image contrast loss can be restored using image processing techniques.

- Improvement in the image acquisition and processing

  Digital radiography allows image acquisition without waiting for the film processing, and the use of digital processing techniques through the application of sophisticated algorithms, like contrast change, equalization and image subtraction [14], this last one very important for the detection of anomalies in the tissues.

- Image acquisition, visualization, storage and recovery ease

  The image acquired will be displayed in a screen instead of a film, and can be stored in databases which make it easier to recover and transmit it.

These characteristics and possibilities have led to an increased use of radiology in other scientific fields (e.g. astrophysics, radiochemistry) and in security applications.

2.2 Detection Methods

There are two main methods to detect and acquire X-rays, known as direct and indirect method [2]. X-rays detectors are divided in these two methods according to the approach used in the conversion of X-rays into electric signals.

The direct method normally uses highly radiation absorbent photoconductive materials that are directly exposed to the X-rays. However, due to incompatibilities between processes, the readout electronic circuit must be developed in separate. Moreover, a high voltage is necessary to operate these devices [3].

The indirect method is based on the use of scintillators, materials that absorb X-rays and converts its energy into visible light [3]. These materials are placed on the top of photodetectors that convert visible light into electrical signals. Despite of its simplicity, this configuration faces limitations regarding the spatial resolution due to scintillator thickness constraints [2]. As the scintillator thickness increases, the absorption of X-rays also increases, but the spatial resolution decreases (Figure 4).

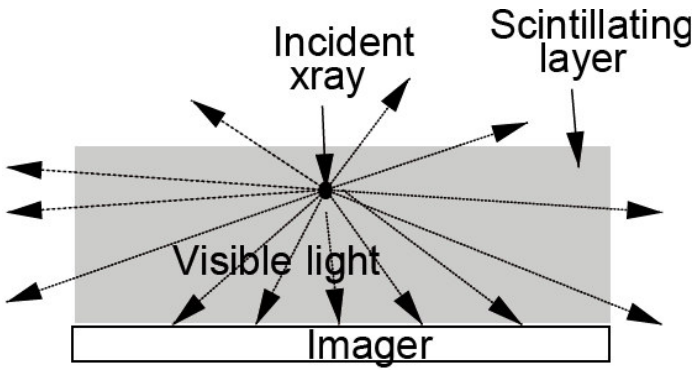

Figure 4. X-ray detector representation with a scintillating layer [15]

Figure 5 shows the differences between the configurations of X-ray detection by Direct and Indirect Method.

In both methods the detectors are developed on rigid substrates (usually silicon plates) [3], and it is necessary to place many of them in an array disposition to obtain an X-ray image [16]. These factors can be considered a drawback for some application that require a flexible and/or large detection system.

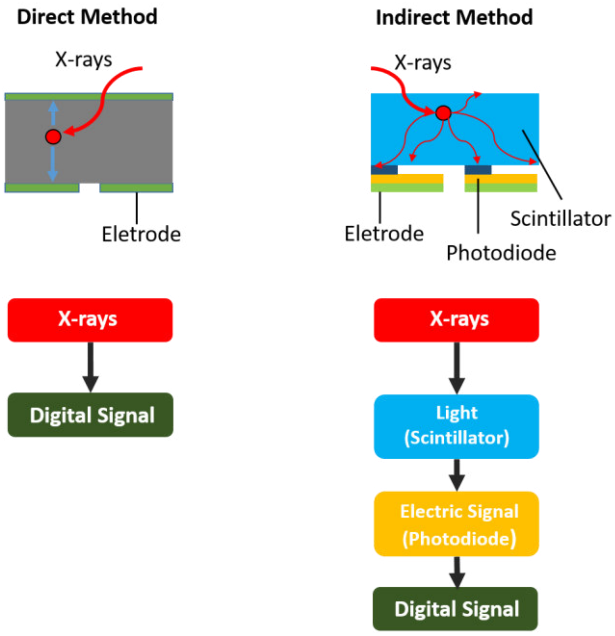

Figure 5. Differences between direct and indirect method of acquiring the X-ray signal [10]

2.2.1 Selected Detection Method

The aim in this work is to design an X-ray detector that can overcome conventional limitations that radiography has to face, like large and/or flexible detection areas.

Nowadays, printed electronic components allow the development of flexible electronic systems or the production of large detection areas at a low price.

The development of a polymer-based scintillator will also meet the characteristics needed to design the detector.

Thereupon, the method to be followed in this work, in order to respond to the objectives and achieve all the characteristics and properties desired, will be the indirect method.

2.3 Scintillator Materials

Scintillator materials started to appear in the beginning of 20th century. Firstly, used in radiation counters, their use gained popularity after the invention of photomultiplier tubes and photodiodes

[17]. Nowadays, scintillators are used in many applications such as digital X-ray detectors, luggage inspection devices, high energy physics, among others [18-21].
There are some necessary properties and characteristics to take in account for the practical use of a scintillator [22, 23]:

- High efficiency, in order to effectively convert the absorbed energy, enabling the radiation dose reduction;

- Proportional linearity between absorbed energy and the number of generated photons;

- Short decay time of the material, which implies a short emission period allowing a correct and precise particles count.

The scintillator efficiency has a high importance in order to reduce the radiation dose applied. The scintillator spectral zone is another very important property, since the scintillator emission spectre must coincide with the photodiode detection zone.
According to these properties it is possible to classify the scintillators in different categories: organic crystals, inorganic crystals, liquids, plastics, glasses and gas [22].

Some scintillators and its characteristics are represented in Table 1.
The abbreviations in Table 1 represent: density (ρ), atomic number (Z_{eff}), generated light (L_R), emission wavelength (λ) and scintillation decay time (τ).

The most used scintillator materials are the organics and inorganics crystals [24]. Organic scintillators have fast-response but have less efficiency, while inorganic scintillators have limitation on response time but have better radiation output and linearity [17]. To design X-ray detectors, the most suitable scintillators are the inorganics. These scintillators are constituted by crystal structures and the most used are the halide crystals and alkaline metals like NaI:Tl, CsI:Na and CsI:Tl, due to their better scintillation efficiency, high density and wavelength between 400 and 600 nm [25, 26].

Table 1 - Some scintillator properties [24, 25]

Scintillator Material	ρ (g/cm³)	Z_{eff}	L_R (phot/MeV)	λ (nm)	τ (ns)	Principal Advantage	Principal Disadvantage
Halides							
TlCl:I	7.0	74.8	~1000	465	200	High ρ and Z_{eff}	Low L_R
NaI(77 K)	3.67	50.8	76000	303	60	High L_R + short τ	Hygroscopic
NaI:Tl	3.67	50.8	43000	415	230	High L_R + short τ	Hygroscopic + non-linear
CsI:Na	4.51	54	43000	420	630	High L_R	long τ
CsI:Tl	4.51	54	65900	560	10^3	High L_R	long τ
CaI_2	3.96	51.1	86000	410	550	High L_R	Very hygroscopic
HgI_2	6.38	68.8	6000	580	2.1x10^3	High ρ and Z_{eff}	Low L_R
Oxides							
$LuAlO_3:Ce^{3+}$	8.34	64.9	11400	365	17	High initial intensity	Small crystals
$Gd_2SiO3:Ce^{3+}$	6.71	59.4	10000	430	56600	High dose resistance	Fragile
$Lu_2SiO3:Ce^{3+}$	7.4	66.4	27000	420	40	High L_R + short τ	Small crystals
$Lu_3Al_5O_12:Sc$	6.7	62.9	22500	270	610	High L_R	long τ
$CdWO_4$	7.9	64.2	19700	495	2-15)x10^3	High ρ and Z_{eff}	long τ
$PbWO_4$	8.28	75.6	~100	~475	~10	High ρ and Z_{eff}	Low L_R
$Bi_3Ge_4O_{12}$	7.13	75.2	8200	505	300	High ρ and Z_{eff}	Low L_R
Chalcogenide							
$Gd_2O_2S:Pr,Ce,F$	7.34	61.1	~40000	511	~3x10^3	High ρ and Z_{eff}	long τ
ZnS:Ag	4.1	27.4	73000	450	10^5	High L_R	Only dust-state
CdS:Te	4.8	48	17000	640	~270-3000	High L_R	Low ρ and Z_{eff}
Glasses							
CsF	4.64	53.2	1900	390	2-4	short τ	Hygroscopic
BaF_2	4.88	52.7	1430	175	0.8	short τ	Low λ
			9500	220	630		long τ
CeF_3	6.16	53.1	4500	330	30	High dose resistance	Low L_R

2.3.1 Polymer Composites based on Scintillator Nanoparticles

The active research for new solutions to overcome limitations and improve the materials application is related with obtaining shorter scintillation decay periods, wider thermal stability, higher flexibility and lower production cost [16, 27, 28]. In order to achieve better energy conversion efficiency, new studies have reported the need to use materials with high atomic numbers. Polymer-composers with scintillator particles come up as a solution and option to be used in radiation detection [28, 29].

Polymeric materials have advantageous characteristics to be used in the experimental and industrial fields. They have high corrosion resistance, low molecular density, low production cost, excellent mechanical properties and easy processing and handling [30].

The development of polymer-composers with the inclusion of scintillator nanoparticles presents new application opportunities due to their combined attractive characteristics: the low production cost of the polymer base of these composers; and the increase of composer density and atomic number, thereby the increase of scintillator efficiency [4]. These materials also offer exclusive characteristics like high flexibility, adequate response time, mechanical and chemical stability and allow large areas fabrication [31, 32]. These characteristics allowed an increasing number of applications such as biomedical materials, functional textile fibres, sensors for radiation detection, energy generation and storage materials, among others.

2.3.2 Selected Polymeric Materials

The polymeric material selection is also very important as it provides the mechanical characteristics desired for the application.

In this work, in order to develop a flexible and stretchable material able to convert X-rays, it is necessary to select a polymer with good mechanical properties, thermally stable and with chemical and radiation resistance. This polymeric material will be used as a binder to hold the scintillator nanoparticles and form a mechanical and chemical cohesive material.

One can select different polymeric materials as polymeric binders, such as the Polystyrene (PS), the Poly(vinylidene Fluoride) (PVDF), the Poly(Vinyl Alcohol) (PVA) and the Styrene-Ethylene/Butadiene-Styrene (SEBS).

PS and PVDF are flexible and stable binder matrices, with high resistance to thermal and light deterioration. While PS have suitable optical properties, showing a high transparency over a wide spectral range ($\lambda > 290$ nm), the PVDF shows low surface tension [33, 34]. PVA presents as its great advantage being biodegradable, since it is water soluble, allowing a green and sustainable chemistry [35]. SEBS offers high levels of stretchability, highly repeatable deformation and chemical resistance [36]

From among these, SEBS was the polymer selected since its characteristics and properties fulfil the composite necessities and the work objectives.

2.3.3 Selected Scintillator

In this work, in order to design the X-ray detector, the emission wavelength of scintillator and the photodetectors selected must comply. Moreover, the scintillator must have the better efficiency possible in accordance with the work objectives.
The scintillator selected in this work is the Europium-doped Gadolinium (III) oxide ($Gd_2O_3:Eu^{3+}$), which characteristics are [5]:

- Efficiency: 20000 photons/MeV
- High Atomic Number
- High density: ~7.4g/cm^3
- Low Scintillation-decay Time: < 2ns
- Emission Wavelength: 611 nm

Besides these attractive characteristics, one of the main advantages of this material is that it can be obtained in nanoparticles, which allows its inclusion in polymer composers.

2.4 Radiation Detection

There are several detection methods, and each one has its own advantages and disadvantages [37]:

- pn Junctions

  This method is usually implemented in amorphous silicon substrates. Electron-hole pairs are created in the pn junction region due to the absorption of X-ray photons, and are subsequently separated by the electric field.

  The main advantage of this method is the low quantity of energy needed to produce one electron-hole pair (a little over 1 eV of energy).

  However, the X-ray absorption power of silicon is much reduced. For example, a 525 μm thickness detector would only absorb 2.2% of 100 keV X-rays (in order to obtain an absorption rate of 50% the detector must have 16 mm of thickness, which is not practical).

- Photoconductors

  This method uses materials (like amorphous selenium) whose conductivity changes with the amount of absorbed radiation.

  These detectors have higher absorption power than silicon (a 525 μm thickness detector would absorb approximately 12.7% of 100 keV X-rays) but need 50 eV to produce an electron-hole pair and a high bias voltage to operate properly (about 10 V/μm) [38].

- Thermal effects

  The working principle of this method is based on the Seebeck effect, that consists in detecting the increase in temperature caused by the absorption of X-rays by a material with high atomic number and high density. To detect the temperature change it is used two thermoelectric materials with different Seebeck coefficients [3].

  A bias voltage is not necessary since the output signal appears as an electric voltage. However, the frequency response is very reduced, of the order of tenths of Hz. Figure 6 shows the basic structure of such detector.

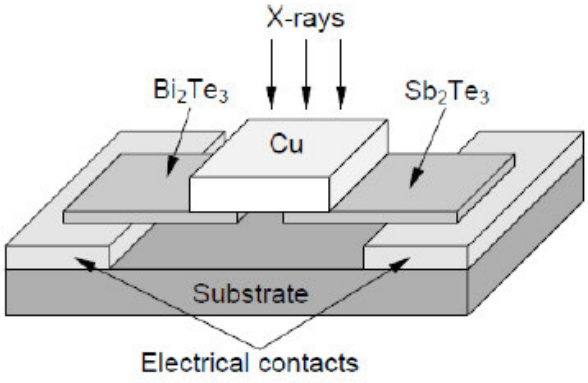

Figure 6. Structure of an X-ray detector based in thermal effects, using Sb_2Te_3 of p type and Bi_2Te_3 of n type as thermoelectric materials [3]

2.4.1 X-Ray Detectors based on Scintillators

X-ray detectors use a scintillator, a material that converts the energy of the radiation absorbed into visible light. Then, the visible light is detected by a photodetector and converted into an electrical signal. The scintillator material must be constituted by elements of high atomic numbers and high density in order to have a better radiation absorption capability [4].

Figure 7 shows the structure of an X-ray image detector based on scintillators.

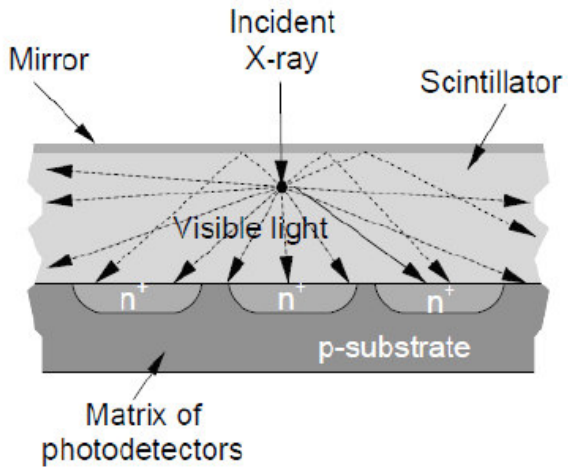

Figure 7. Basic structure of X-ray detector based on scintillators [2]

Scintillators have high X-ray absorption power and high frequency responses (usually in the GHz range) without the need for bias voltage [37].

However, restrictions imposed by the height of the scintillator are going to result in some limitations in spatial resolution. Increasing the height of the scintillator increases the number of X-ray photons absorbed but the amount of light that reaches neighbourhood pixels will also be higher, thus decreasing spatial resolution [39].

Using an individual scintillator for each photodetector pixel, separated by layers of a reflection material, allows the increase of spatial resolution without decreasing the height of the scintillator, as it is shown in Figure 8 and Figure 9 [40].

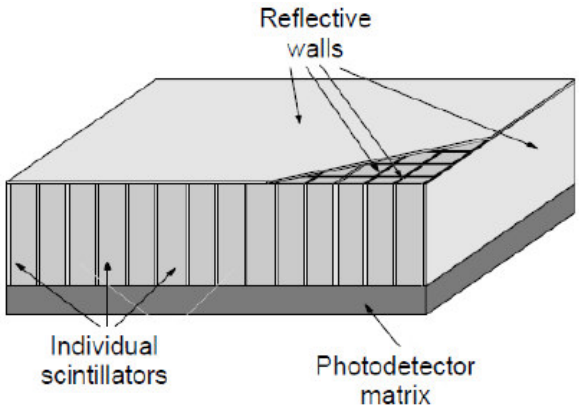

Figure 8. Schematic representation of a structure based on an individual scintillator for each photodetector [2]

Figure 9 shows a schematic of a detector where aluminium is used as reflective material and the scintillator (thallium doped cesium iode, CsI:Tl) is divided for each detection pixel.

The aluminium layer allows the penetration of X-rays due to its low atomic number and density while its high reflectivity for visible light guides it to the corresponding photodetector.

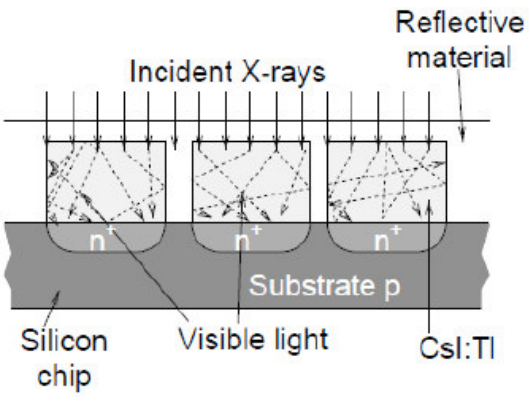

Figure 9. Schematic diagram of an X-ray imaging detector based in scintillators [2]

During this process, some critical steps that can influence the efficiency and the noise in the signal must be taken in account [2, 37, 41]:

- Transmission of X-rays through the reflective layer

  The absorption of beams by some material occurs according to the Lambert-Beer law [41]:

  $$I = I_o e^{-\mu x} \qquad (a)$$

  where I is the intensity of the beam, I_o is the initial intensity of the beam and μ is the coefficient of the material's linear absorption.

  Through this equation it can be concluded that the higher the thickness of the reflective layer, the lower the radiation transmission ratio. Figure 10 shows the relation between the aluminium layer thickness and the transmissivity of X-rays.

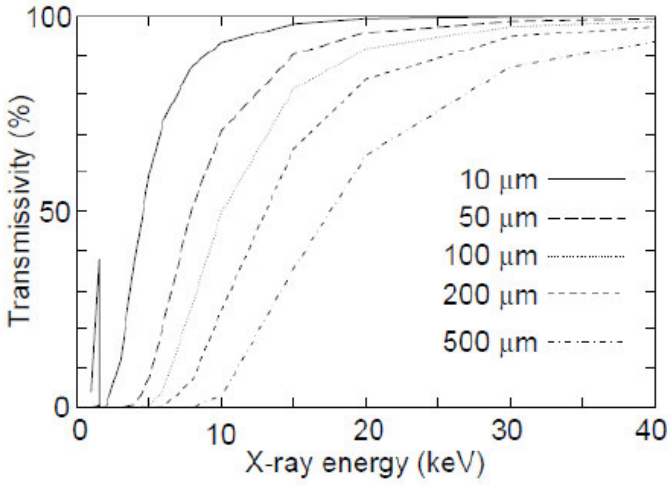

Figure 10. Transmissivity of X-rays of different aluminium thickness [41]

As it can be observed, the transmissivity decreases with the increasing of the layer between 10 μm to 500 μm.

- Absorption of X-Rays by the Scintillator and Their Conversion into Visible Light

  The absorption of X-rays by the scintillator depends also on equation (1). However, the mass absorption coefficient must be calculated separately for each element that form the

different composites in the scintillator, using equation (2), where α is the fine-structure constant and Z is the atomic number [37].

$$\sigma_{pair} \approx \frac{7}{9} 4\alpha r_e^2 Z^2 \ln\left(\frac{183}{Z^2}\right) \quad (b)$$

Figure 11 shows the relation between the CsI:Tl scintillator thickness and the absorption ratio. As expected, the X-ray absorption increases with thickness.

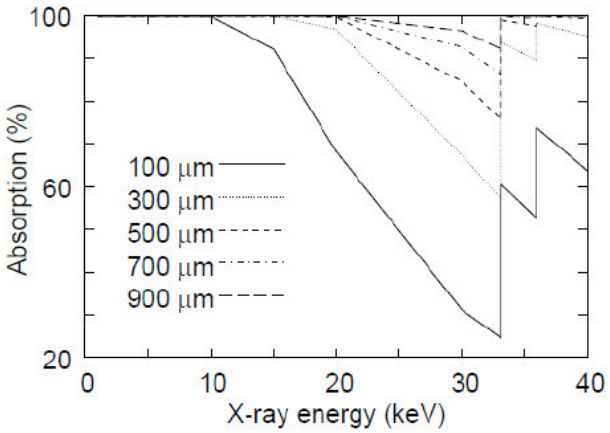

Figure 11. Absorption of X-rays by CsI:Tl scintillators of different thickness [41]

- Reflection of Visible Light by the Reflective Layers

  The reflectivity between scintillator and a homogeneous metallic reflector is given by [37, 42]:

$$R = \left|\frac{u_{SC} - u_R}{u_{SC} + u_R}\right|^2 \quad (c)$$

where u_{SC} and u_R represent the refractive indexes of the scintillator and the reflector respectively.

In case of a reflector with multiple interfaces, the generalized index of the film placed between the scintillator and the reflector wall is represented by u_i, and in this case the Snell Law is applied:

$$u_{SC} \sin\theta_{SC} = u_i \sin\theta_i = u_W \sin\theta_W \quad (d)$$

where *w* represents the reflector wall. In this instance, the reflectivity is given by:

$$R = |r|^2 = \left|\frac{Eq^-}{Eq^+}\right|^2 \quad (e)$$

where Eq^- and Eq represent the amplitudes of electric field vectors of the incident and reflected waves, respectively.

- Transmission and Guidance of the Visible Light to the Photodetector

  Some light produced by the scintillator is reflected in the surface of the photodetector due to differences of refractive indexes between them.

  To reduce this phenomenon, it may be necessary the use of an antireflective filter. The simplest way to obtain it is applying a thin film in the surface of the photodetector [41].

  For a reflectivity equal to zero, the following equation is given:

$$R = \left|\frac{E_{sc}^-}{E_{sc}^+}\right|^2 = 0\ (=)\ u_{sc}u_{ph} = {u_{tf}}^2 (=)\ u_{tf} = \sqrt{u_{sc}u_{ph}} \quad (f)$$

  being u_{sc}, u_{ph} and u_{tf} the generalized refractive indexes of the scintillator, the photodetector and the thin-film, respectively.

  It is not easy to find an adequate material according to the equation (6). However, there are some good option to antireflective film, such as SI_3N_4, ZrO_2, TiO_2 with refractive indexes of 2.01, 2.22 and 2.94, respectively [37, 43].

  Due to the multiple reflections, the light reaches the photodetector already with losses. Changing/increasing the size of the photodetector pixel can improve the efficiency of the system. However, it must be taken in account the remaining system geometry [2].

- Direct Detection of X-rays by the Photodetector

  Some X-ray photons are absorbed by the photodetector after crossing completely the scintillator layer. To calculate the noise ratio associated with this absorption, one usually applies the Monte Carlo method [44].

2.5 Photodetection Technologies

Light is transduced into an electric signal by photodetectors whose are constituted by a matrix of pixels that will convert the light into electrons. This electron generation is dependent and proportionally linear to light intensity [45].
Nowadays there are two types of technology used in the imaging field applications:

- Charge Coupled Device (CCD);
- Complementary Metal Oxide Semiconductor (CMOS).

It is essential to analyse the characteristics of both technologies in order to make a careful selection that fulfil all the requirements, such as dimension, resolution and low cost.

2.5.1 Charge Couple Devices

The CCD was invented in 1970 at Bell Laboratories by Willard Boyle and George Smith [46]. CCD sensors consists in an array or matrix of pixels (or light sensitive cells) capable of generating electrical charge proportional to light intensity. A CCD pixel is formed from a biased p-n junction, and the incident light generates electron-hole pairs in the depletion region. [47].
CCDs sensors can be developed in different architectures, the most used being: Interline-Transfer, Full-Frame and Frame-Transfer [48].

Interline-Frame: Between the column of pixels there are storage columns (Figure 12). During the integration period (frame capture period), an image is projected on the photoactive matrix, generating an electrical charge proportional to light intensity in each location. These charges are rapidly transferred to the corresponding columns, and then to the Shift Register to be processed one line at a time [47, 48].

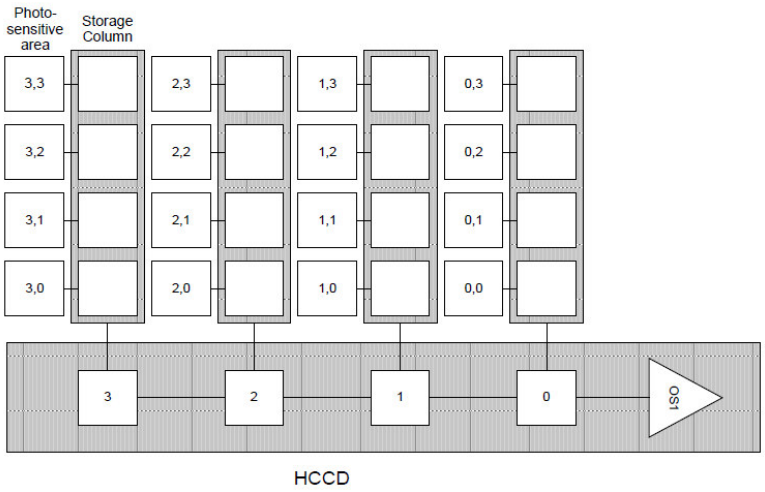

Figure 12. Interline-Frame CCD Architecture [48]

The Interline-Transfer architecture's advantages and disadvantages are [47-49]:

Advantages:

- Fast Actuation, due to the fast charge transfer to the storage columns;
- Low-cost: A huge amount of the image sensors industry uses Interline-Transfer sensors, which leads to mass production and, consequently, price reduction.

Disadvantages:

- Low Fill Factor: approximately 30%. The sensor is subject to aliasing (image distortion effect) since it is not fully photo-sensible due to the storage areas;
- Need for lenses to increase the fill factor and reduce the aliasing.

Full-Frame: The imaging area is fully photoactive, not existing storage areas like in Interline sensors (Figure 13). After the integration period, the generated charges are transferred one line at a time to the Shift Register, where it will be processed to form the frame [50].

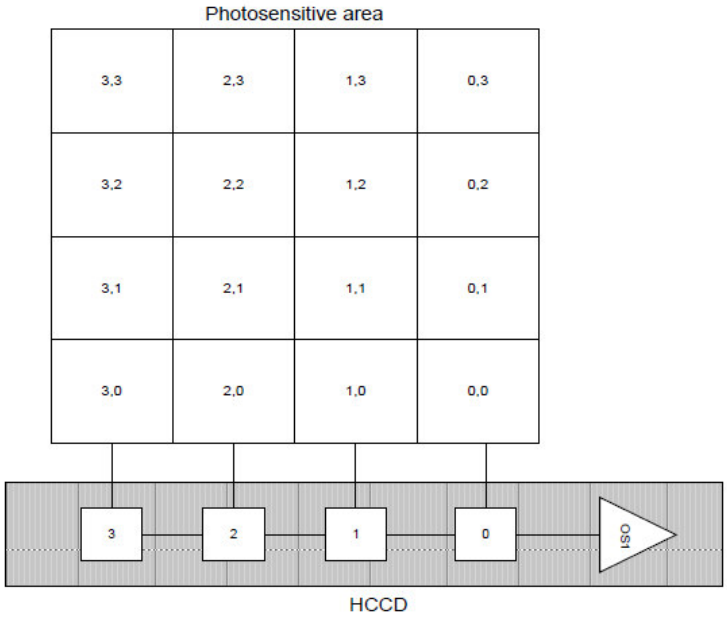

Figure 13. Full Frame CCD Architecture [48]

The Full-Frame architecture's advantages and disadvantages are [48, 50]:

Advantages:

- Total Fill Factor (100%), since all the imaging area is photo-sensible;
- Low Aliasing: since the fill factor is equal to 100%, the frames will suffer very low distorting in relation to the captured image;
- Wide array of resolutions and frame rates.

Disadvantages:

- Use of a shutter: During the transfer period of the generated charges to the Shift Register, the non-processed pixels can still capture incident light that can lead to a lag in the frame. It is necessary to block the sensor (usually using a mechanical shutter) or the light source (a highly complex process, sometimes even impossible).

Frame-Transfer: Like Full-Frame sensors, the imaging area is fully photoactive. After the integration period, the generated charges are rapidly transferred to a non-photoactive storage area of the same size (Figure 14). Then the frame is processed from this area while the new integration period begins [49, 50].

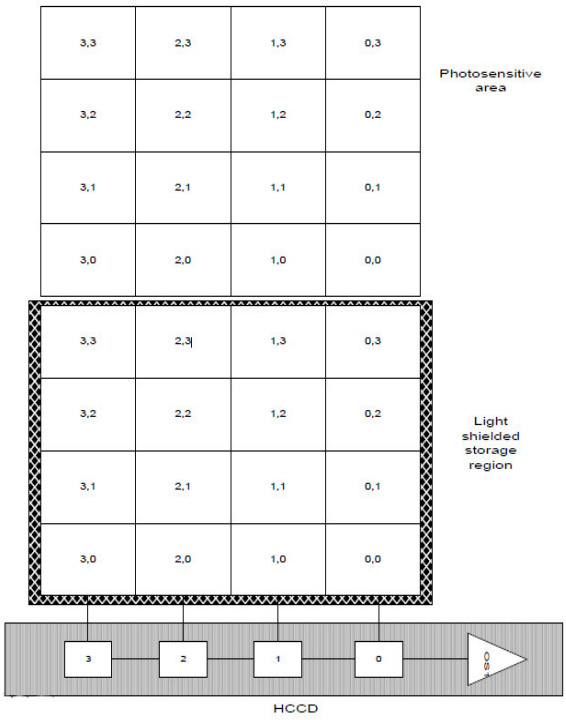

Figure 14. Frame-Transfer CCD Architecture [48]

The Frame-Transfer architecture's advantages and disadvantages are [48, 49]:

Advantages:

- Total Fill Factor (100%), since all the imaging area is photo-sensible;
- Low Aliasing: since the fill factor is equal 100%, the frames will suffer very low distorting in relation to the captured image;
- Shutter-free: since the generated charges are rapidly transferred to the storage area, it is not necessary to block the light.

Disadvantages:

- Dimension: As it is necessary two matrices of the same size, the Frame-Transfer sensor will be, at least, double the size of a Full-Frame sensor;
- Higher cost, since more materials (e.g. silicon) are needed to produce these sensors.

2.5.2 Complementary Metal Oxide Semiconductor (CMOS)

The CMOS was patented in 1963 by Frank Wanlass while working for Fairchild Semiconductor [51].

The architecture of CMOS imaging sensors can be divided into four principal sections [52]:

- Photoactive pixels matrix;
- Analog signal processors;
- Column and line selection system;
- Timer and control system.

Like CCDs, the CMOS sensors are formed by a matrix capable of generating electrical charges proportional to the incident light, but the light acquisition process is very different, since each CMOS pixel employs a photodiode, a capacitor and transistors.

The capacitor will be charged before the integration period begins. As this period begins, the charge in the capacitor will slowly drain through the photodiode, proportionally to the incident light. The remaining charge at the end of the integration period will be readout and digitised [47].

There are two types of CMOS sensors: Active Pixel Sensor (APS) and Passive Pixel Sensor (PPS) (Figure 15).

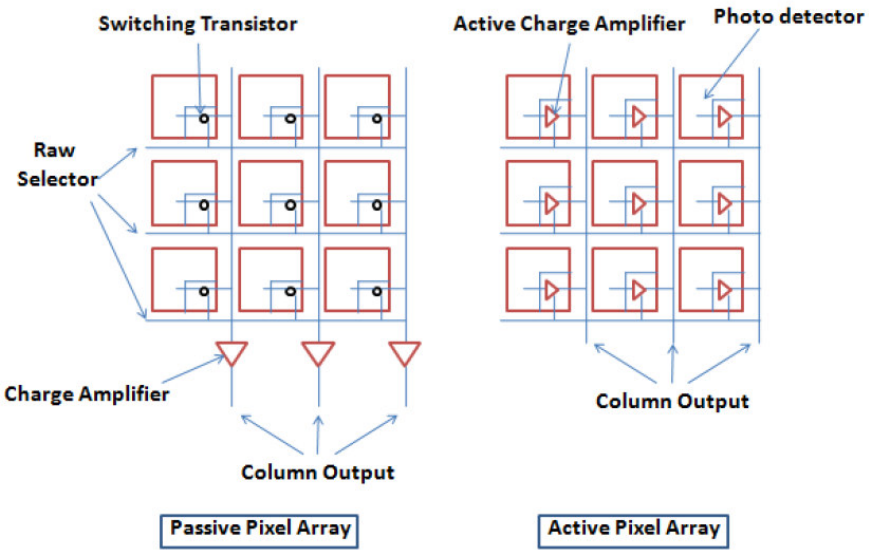

Figure 15. Passive Pixel and Active Pixel CMOS architectures [45]

The main difference between these two architectures is related to the amplifier position: in the PPS the amplifiers are located at the end of each column while in APS they are implemented in each pixel [45].

CMOS sensors have many advantages like low cost and less power consumption but also present some drawbacks and performance limitations in image quality [45, 52]:

Advantages of CMOS sensors

- Low Cost Production;
- Low Power Consumption
- High Imaging Velocity, allowing the image capture in short periods.

Disadvantages of CMOS sensors

- Low Fill Factor: The imaging area is not all photoactive, especially in the APS;
- Low Sensibility, which is related to the fill factor and photon generation rate;
- Noise susceptibility;
- Limited Dynamic Range.

2.5.3 Differences Between CCD and CMOS sensors

The main difference between CCD and CMOS system architectures is related with the integration of companion functions.

Figure 16 shows that CMOS technology, contrarily to CCD, allows the integration of the pixel array alongside all the complementary electronics need to process and digitise the signal.

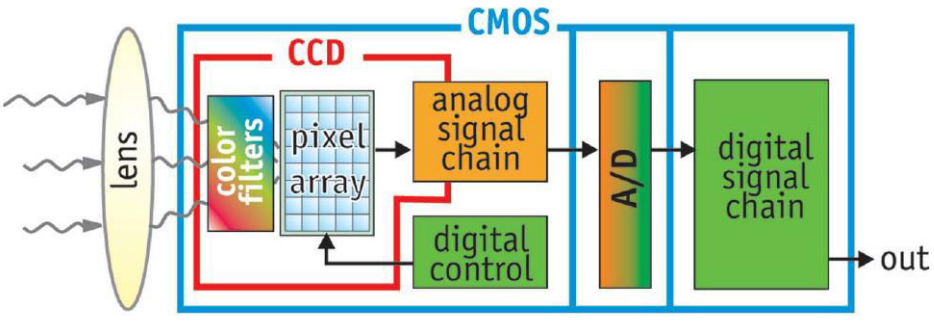

Figure 16. Difference between CCD and CMOS system architectures [53]

The integration of all the companion functions will allow CMOS systems to be more compact, lighter and consume less power when compared to CCD systems.

Table 2 summarizes the main advantages of both technologies when compared to each other.

Table 2 - Summary of the main advantages of CCD and CMOS image sensors [52]

CCD	**CMOS**
Lower noise	Low power consumption (~100x less)
Smaller pixel size	Single power supply
100% Fill Factor	High integration capability
Superior image quality	Lower cost
Low dark current	Single master clock
Higher sensitivity	Random access
Electronic shutter without artefacts	Flexibility

2.5.4 Photodetectors based on CMOS technology

In order to develop and design a sustainable, flexible and/or large detection system, the photodetectors selected in this work are the CMOS photodetectors.

CMOS photodetectors have many advantages that meet the characteristics and properties desired to the final detection system, such as [52]:

- Flexibility
- High integration
- Low cost
- Low power consumption and one single supply

These characteristics, along with the scintillator selected, will allow to design a detection system able to fulfil the objectives of this work.

3. DEVELOPMENT OF SCINTILLATOR-BASED POLYMER NANO-COMPOSERS

3.1 Introduction

Conventional indirect radiation detectors have several drawbacks since scintillators have limited efficiency, light yield, flexibility, response time and present a high cost production [32, 54].
To develop indirect radiation detectors able to overcome these limitations, flexible polymer matrix with dispersing scintillating nanoparticles have been researched and prepared [55, 56].
The polymer matrix provides a short scintillation time when compared to current available scintillators [28]. However, its low production cost and versatility led to seek different approaches and novel materials [57].

Polymer-based scintillator nanocomposite research has increased significantly and attracted more attention due to their interesting properties, such as scintillation decay time, thermal stability, flexibility, low cost and large area fabrication ease [4, 28]

A novel composite based on gadolinium oxide doped with europium ($Gd_2O_3:Eu^{3+}$) and fluorescence molecules 2,5-dipheniloxazol (PPO) and (1,4-bis (2-(5-phenioxazolil))-benzol (POPOP) will be characterized and used to efficiently convert X-ray radiation into visible light [33].

3.2 Scintillator Preparation

3.2.1 Materials Selected

$Gd_2O_3:Eu^{3+}$ nanoparticles present very interesting properties to be used as a scintillator due to their wide band gap (~5.2 eV), atomic number, high density (~7.4 $g.cm^{-3}$), suitable light yield (~2×10^4 $photons.MeV^{-1}$) and radioluminescence [58]. To further improve the overall visible light yield resulting from the X-rays conversion, this scintillator is incorporated with fluorescence molecules PPO and POPOP [5].

The polymer matrix selected is from the elastomer styrene-butadiene-styrene (SBS) family. These materials show highly repeatable deformation and chemical resistance [59] but its poor biostability is a huge obstacle to their application in the biomedical area.

The SBS family are thermoplastic elastomers (TPE), materials that combine the properties of rubbers and thermoplastics, and present large deformation, flexibility and optical resistance [60].

The Styrene-Ethylene/Butylene-Styrene (SEBS) is a co-polymer from the TPE family. It presents lower butadiene ratio and an efficient and stable binder with high biostability, allowing it to be used in biomedical applications [36]. Furthermore, SEBS presents an excellent radiation and temperature resistances, and good mechanical and optical properties [58].

3.2.2 Sample Preparation

Homogeneous samples were developed preparing the different components: SEBS nanoparticle films with thickness of ≈ 50 μm, $Gd_2O_3:Eu^{3+}$ nanoparticles content ranging from 0.25 to 0.75 wt.%, and concentrations of 1 wt.% of PPO and 0.01 wt.% POPOP fluorescent molecules [61].

3.3 Printing Technologies

In the last decade it was noticed a significative evolution in printed electronic technologies.

There are many printing techniques, and the most widely used are Screen Printing, Spray Printing and Inkjet. These techniques allow the development of printed electronic components from ink with polymer-based nanocomposers, which present very attractive characteristics like low cost, adaptability, wide area and high-speed production, high resolution and miniaturisation of devices [62].

3.3.1 Screen Printing

Screen Printing is a technique used since the middle of 20th century in the textile industry, and has been adapted to allow the use of functional inks in flexible materials and substrates [63] .

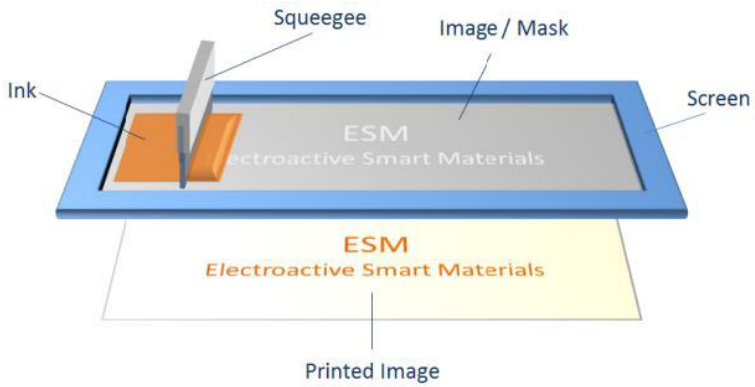

Figure 17. Screen Printing schematic representation [64]

In this printing process, firstly, the ink is spread through the screen and the mask (Figure 17). Using a squeegee, and due to the mask geometry, the ink will be deposited on the desired location of the substrate. Lastly, to guarantee the adherence, the substrate with the deposited material undergo through a thermal cure.

The good quality-price relation, reproducibility, scaling, simplicity and multi-materiality make this technique very suitable to nanocomposite printing [65].

3.3.2 Spray Printing

Spray Printing is an economic and efficient technology used widely in humidification, surface coating and automobile industry [66].

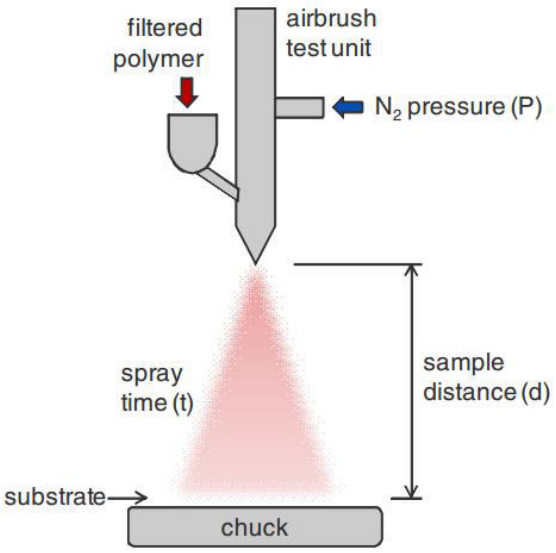

Figure 18. Spray Printing schematic representation [66]

As shown in Figure 18, in this technique a pulveriser is used to deposit the material. The pulveriser will spray the ink homogeneously using a pressurized gas. To regulate the viscosity of the ink deposited it is necessary to adequate the gas pressure while the humidity and homogeneity are related to the distance between the substrate and the pulveriser. A smaller distance between substrate and the pulveriser will result in an higher humidity and lower homogeneity while a bigger distance will result in a more homogeneous but dryer deposition [66].

This technology process is simple and fast, compatible with flexible substrates, allows the thickness adjustment and presents low cost production to large organic electronics areas [66-68].
However, this technology have some drawbacks such as low level of homogeneity, low resolution and an extremely high surface roughness [66].

3.3.3 Inkjet Printing

Inkjet printing is a digital technique that was first developed in the early 1950s [69]. Since then, this technology progress has allowed a significant improvement in printing resolution and speed, gathering attention towards its use as a technique to print electronic components, like organic light-emission diode (OLED), liquid crystal tunable filters (LCTFs) or organic transistors [68].
Being a digital printing technique, it allows for a fast design and scale change, which is a great advantage in small and medium volumes production [67]. This process also allows ink injection

without contact and printing onto flexible subtracts [70] while consuming less deposition material, which leads to a lower cost production [68].

This technology can be used through various methods, and the more relevant are the Continuous Mode, the Thermal and the Piezoelectric Drop-On-Demand (DOD).

In the Continuous Mode (Figure 19), the ink is pumped through a printing nozzle in order to obtain a liquid jet. Through a periodic interruption of the jet, evenly spaced drops of the same size can be obtained. This method is mainly used when printing speed is essential [71].

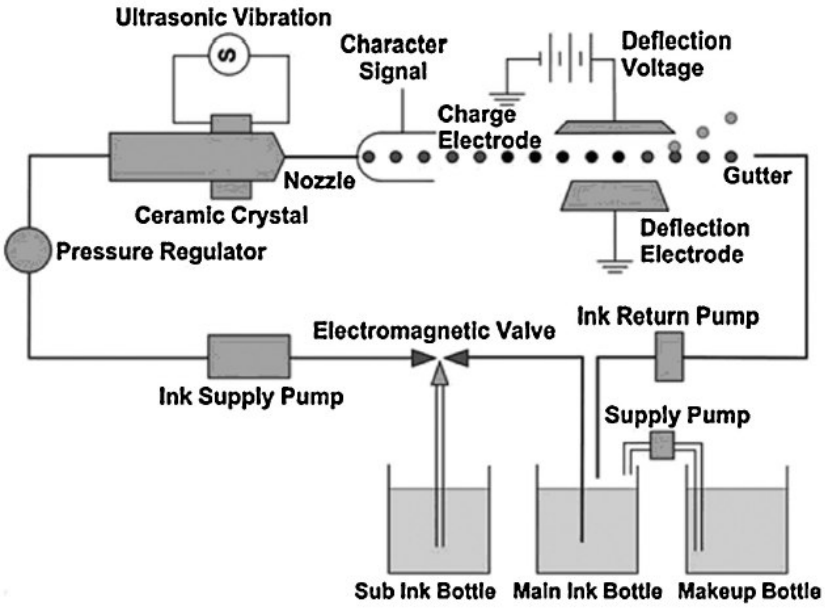

Figure 19. Continuous mode inkjet printer [71]

Both DOD methods allow smaller drops, better resolution and less ink property limitations.

In Thermal DOD, a heating resistor raises the ink's temperature, forming a vapour bubble that forces out an ink drop (Figure 20). However, this method is restricted to aqueous systems [71].

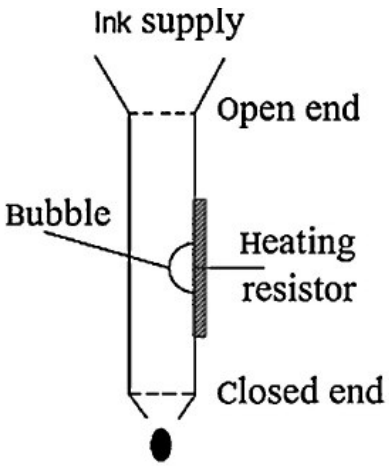

Figure 20. Thermal DOD inkjet printing [71]

In Piezoelectric DOD, the ink drop is forced out due to an acoustic pulse generated by the deformation of a piezoelectric membrane (Figure 21). Since there is no need for a temperature variation, this method is compatible with a wide range of solvents [71].

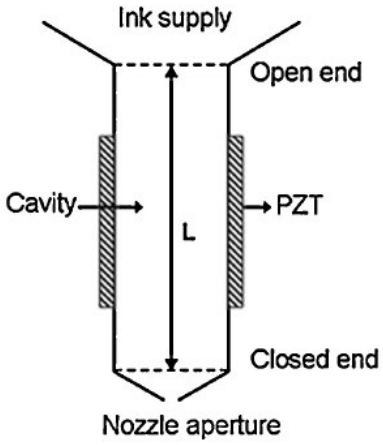

Figure 21. Piezoelectric DOD inkjet printing [71]

4. Development of an Electronic System for Visible Light Detection

4.1 Introduction

The possibility of utilizing polymer-based scintillator nanocomposites on radiation detection creates a need for developing an electronic system to complement their function.

The scintillator's function is to convert the incident X-rays into visible light. To process this visible light, it is necessary a system able to detect light and acquire the resultant data, handle this data, and display the final results.

Figure 22 represents the Block Diagram of the system to be developed in this work.

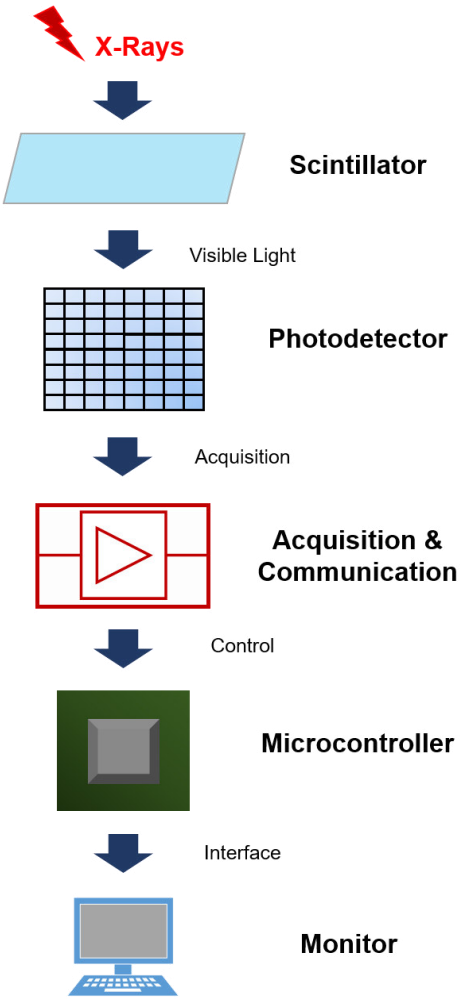

Figure 22. System Block Diagram

This chapter will feature the presentation and discussion of a solution to develop a photodetector-based circuit, to detect the light, and the remaining system to acquire and process the collected data.

4.2 Photodetectors

The goal of this system is to detect the light converted from the X-rays by the scintillators. Thereupon, it must be taken in account the scintillator's light output characteristics, in order to select an adequate photodetector.

- Scintillator's emission wavelength (λ) = 611 nm.

For this reason, the selected photodetector must have a light range able to detect a wavelength equal to 611 nm.
Besides that, it must be a CMOS photodetector, due to their high integration, low power consumption and low cost.

4.2.1 Photodetector TSL 235 by Texas Instruments

After an analysis and research for adequate commercial photodetectors, it was selected the TSL235 by *Texas Instruments* (Figure 23) [72].

Figure 23. TSL235 Light-to-Frequency converter by *Texas Instruments*

The TSL235 corresponds to a light-to frequency converter combining a silicon photodiode and a current-to-frequency converter on a single monolithic CMOS integrated circuit (IC) [72]. It is offered in a three-leaded package, as it is shown in Figure 24.

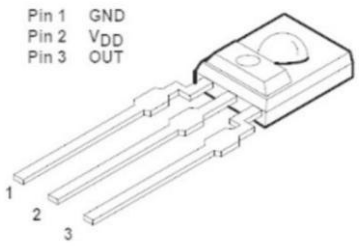

Figure 24. TSL235 three-leaded package. Pin 1: GND, Pin 2: V_{DD}, Pin 3: OUT [72]

The TSL235 principal characteristics are [72]:

- Single-supply Operation down to 2.7V;
- Light Range Detection: 300 nm to 1100 nm;
- Compact Package:
  - Package area: 76,15 mm^2;
  - Photodiode area: 1.36 mm^2;
- Communication directly with the Microcontroller (MCU);
- Non-linearity Error Typically 0.2% at 100 kHz.

These characteristics represent some advantages in using the TSL235. The characteristics "Single-supply Operation" and the "Communication directly with the Microcontroller" permit the simplicity of the circuit while enabling the utilization of low tensions in the system. The "Light Range Detection" cover wide range of wavelengths, and a compact package allow multiple areas and design solutions to the system.

Despite these advantages, it is necessary to compare the TSL235 characteristics to the characteristics applied by the scintillator and the system objectives. This comparison is shown in Table 3.

Table 3 - Comparison between the required and the TSL235 characteristics

Scintillator & System Objectives	**TSL235 by Texas Instruments**
Emission wavelength (λ) = 611 nm	Wavelength detection: from 300 nm to 1100nm
High integration	Compact Package
	Communication directly with MCU
	Single-supply operation down to 2.7V
Low power consumption	

In this comparison it is verified that the TSL235 is a suitable photodetector for the system and that some characteristics fulfil more than one characteristic required by the system.

Additionally, the TSL 235 presents operating characteristics that are important to project and design all the electronic system, with the acquisition and communication circuits, such as the supply voltage and current and the output and full-scale frequency. These characteristics can be observed in Table 4.

Table 4 – Recommended operating conditions and electrical and operating characteristics of TSL235 [72]

Recommended operating conditions	**MIN**	**NOM**	**MAX**	**UNIT**
Supply voltage, V_{DD} (V)	2.7	5	6	
Operating free-air temperature range, T_A (°C)	-25		70	

Characteristics at VDD = 5 V, TA = 25°C		**MIN**	**TYP**	**MAX**	**UNIT**
Supply current, I_{DD}			2	3	mA
Output frequency, f_O (°C)	E_e = 375μW/cm², λ_p	200	250	300	kHz
	E_e = 0		0.25	10	Hz
Full-scale frequency		500			kHz

In the Figure 25 the functional block diagram of TSL235 is represented. The light is detected by the photodiode that converts it into current which is converted into the output frequency. Then, the output frequency can be measured or communicated to a MCU.

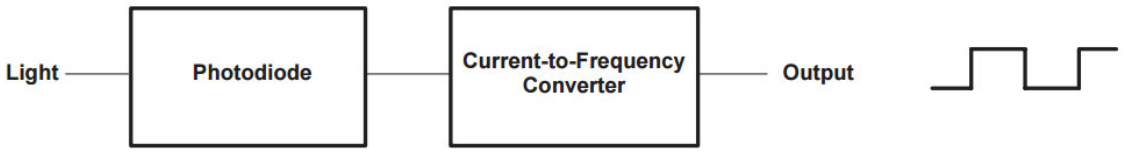

Figure 25. TSL235 Functional Block Diagram [72]

A single TSL235 is able to interface directly with a MCU since its output is frequency. A typical TSL235 interface with a MCU is shown in Figure 26.

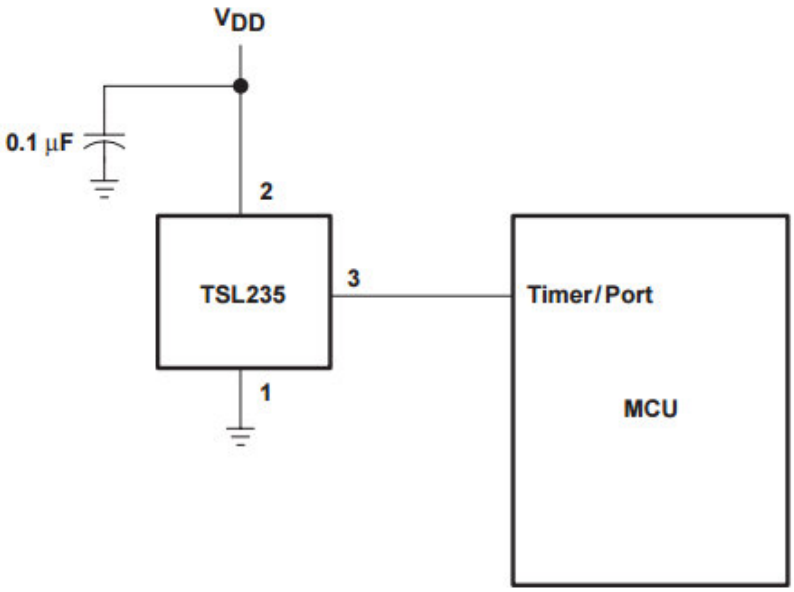

Figure 26. Typical TSL235 Interface with a MCU [72]

In this circuit, the V_{DD} must have a value between 2.7 and 6V, as shown in Table 4, and a capacitor with a value between 0.01 and 0.1µF is used to decouple the power-supply lines in order to optimize the device performance.

However, the interface of a MCU with more than one TSL235 will depend on the number of ports available and in the capacity of the MCU.

4.2.2 Photodetectors Matrix

Besides using and testing a single TSL235, and in order to build a detector that allows a large area detection at a low cost, it will be also projected and designed a matrix formed by TSL235.

To test the proper operation of this approach, the dimension of the matrix to be designed will be four by four (4x4), which means that it will be necessary use 16 TSL235 (Figure 27).

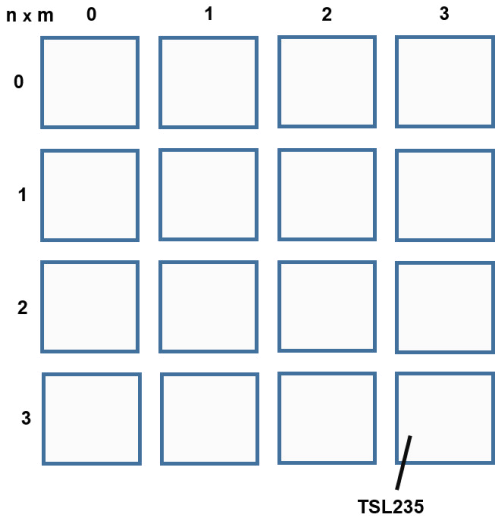

Figure 27. Illustration of a 4x4 TSL235 matrix

This matrix dimension, forming a larger area detection, will be able to detect the presence of small objects when tested.

Figure 28 represents a schematic of the matrix circuit, with the connection between the various TSL235 and the supply voltage (V_{DD}) and the ground. The TSL235 port numeration is related to the pin configuration shown in Figure 24.

The V_{DD} selected to this circuit is 5V since it allows the integration of more components and circuits, being a reference voltage available in many systems. The capacitor value selected is 0.1µF since it has to be between 0.01 and 0.1µF.

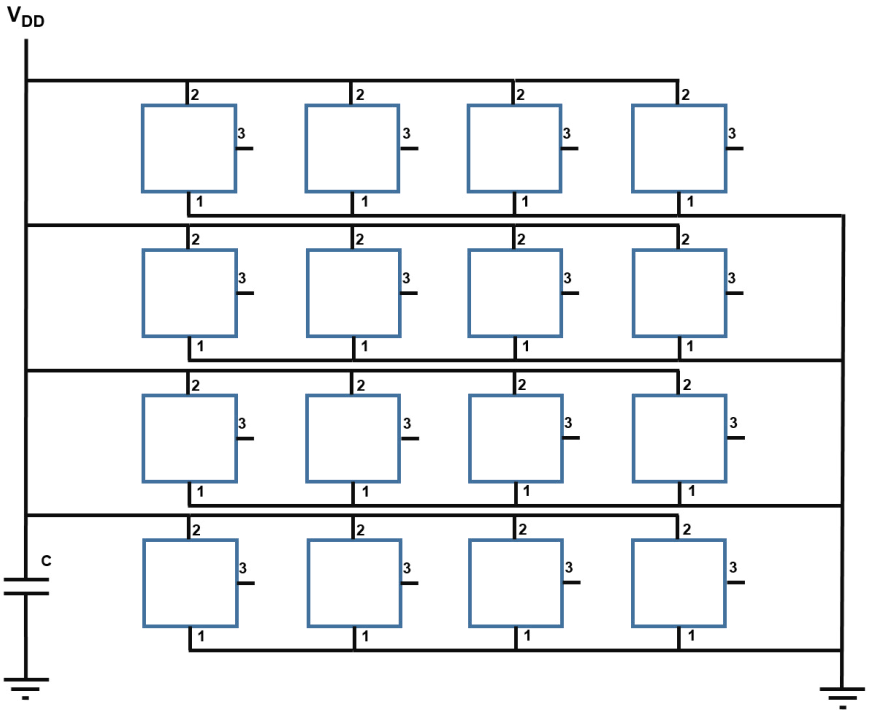

Figure 28. Schematic of the 4x4 TSL235 matrix circuit.

To interface the matrix with a MCU it is necessary to connect directly every TSL235s outputs (port 3) to MCU input ports or to develop an acquisition circuit able to obtain all the signals efficiently.

4.3 Photodetection System

4.3.1 Acquisition and Communication Circuits

There are two different approaches to acquire all the TSL235 output signals: use a MCU with enough input ports to read all of them, or develop a circuit that allows multiplexing all the signals. Due to the low cost and its simplicity, the use of multiplexers, a component able to obtain and multiplex several signals, was the approach preferred.

The multiplexer (MUX) selected to develop the system was the CD4051B by *Texas Instruments*. The CD4051B (Figure 29) is a single 8-channel (8:1) multiplexer/demultiplexer that allows to select the information of eight data sources from a single channel.

Figure 29. CD4051B CMOS Single 8-Channel Analog Multiplexer/Demultiplexer by *Texas Instruments* [73]

The CD4051B principal characteristics are [73]:

- Wide Range of Digital and Analog Signal Levels
  - Digital: 3 to 20 V
  - Analog: ≤ 20 V_{P-P}
- Supply Voltage: -0.5 to 20 V
- Supply Current: -10 to 10 mA

The characteristics referred present several advantages for this MUX to perform the function required, since it presents a wide operation range of signal levels and a supply voltage and current suitable to develop a simpler and low cost consumption system.

The CD4051B pin configuration and functions are shown in Figure 30 and Table 5, respectively.

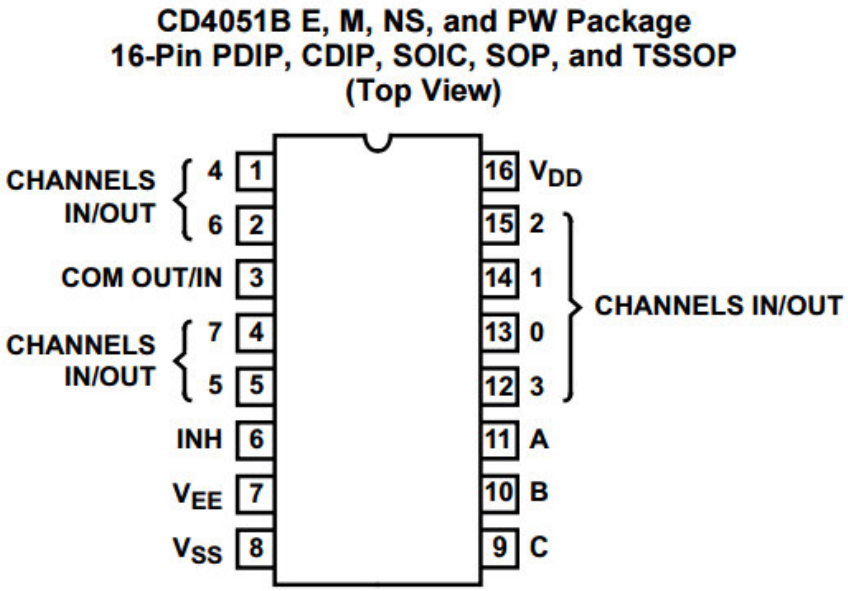

Figure 30. CD4051B Pin Configuration [73]

Table 5 – CD4051B Pin Functions [73]

PIN		I/O	DESCRIPTION
NO.	NAME		
1	CH 4 IN/OUT	I/O	Channel 4 in/out
2	CH 6 IN/OUT	I/O	Channel 6 in/out
3	COM OUT/IN	I/O	Common out/in
4	CH 7 IN/OUT	I/O	Channel 7 in/out
5	CH 5 IN/OUT	I/O	Channel 5 in/out
6	INH	I	Disables all channels
7	V_{EE}	—	Negative power input
8	V_{SS}	—	Ground
9	C	I	Channel select C
10	B	I	Channel select B
11	A	I	Channel select A
12	CH 3 IN/OUT	I/O	Channel 3 in/out
13	CH 0 IN/OUT	I/O	Channel 0 in/out
14	CH 1 IN/OUT	I/O	Channel 1 in/out
15	CH 2 IN/OUT	I/O	Channel 2 in/out
16	V_{DD}	—	Positive power input

There are eight IN/OUT channels (0 – 7) that can be used as inputs channels to read the TSL235 output signals. These input channels can be read/written through three selection channels (A, B and C) whose values combined result in a binary value that corresponds to the selected input channel. Furthermore, there is an inhibit channel (INH) that allows to disable every input channel.

In order to read the sixteen output signals from the 4x4 TSL235 matrix, it is necessary the use of two CD4051B to multiplex all the signals.
Therefore, the photodetectors will be divided so that each one corresponds to a multiplexer input.

Figure 31 represents the TSL235 matrix division in order to be read by two CD4051 (MUX-A and MUX-B).

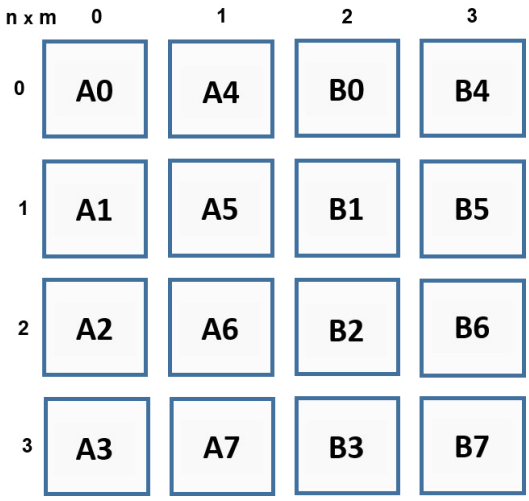

Figure 31. TSL235 Matrix Naming

Each TSL235 is named according to its corresponding IN/OUT channel: the letter corresponds to the multiplexer and the number to the channel in that multiplexer. This correspondence is shown in Table 6.

Table 6 – Correspondence between the CD4051B and the TSL235

Multiplexer MUX-A		Multiplexer MUX-B	
A0	Channel 0 IN/OUT	B0	Channel 0 IN/OUT
A1	Channel 1 IN/OUT	B1	Channel 1 IN/OUT
A2	Channel 2 IN/OUT	B2	Channel 2 IN/OUT
A3	Channel 3 IN/OUT	B3	Channel 3 IN/OUT
A4	Channel 4 IN/OUT	B4	Channel 4 IN/OUT
A5	Channel 5 IN/OUT	B5	Channel 5 IN/OUT
A6	Channel 6 IN/OUT	B6	Channel 6 IN/OUT
A7	Channel 7 IN/OUT	B7	Channel 7 IN/OUT

The Figure 32 illustrates the connection between one CD4051B and the eight sensors correspondent.

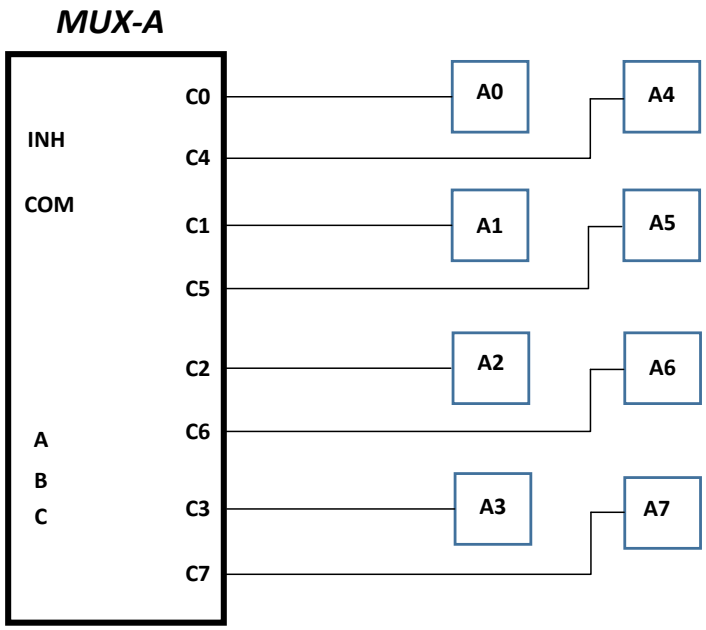

Figure 32. Connection between the MUX-A and the TSL235 correspondents

Figure 33 represents the schematic of the acquisition system, formed by the TSL235 matrix (sixteen sensors) and two multiplexers CD4051B.

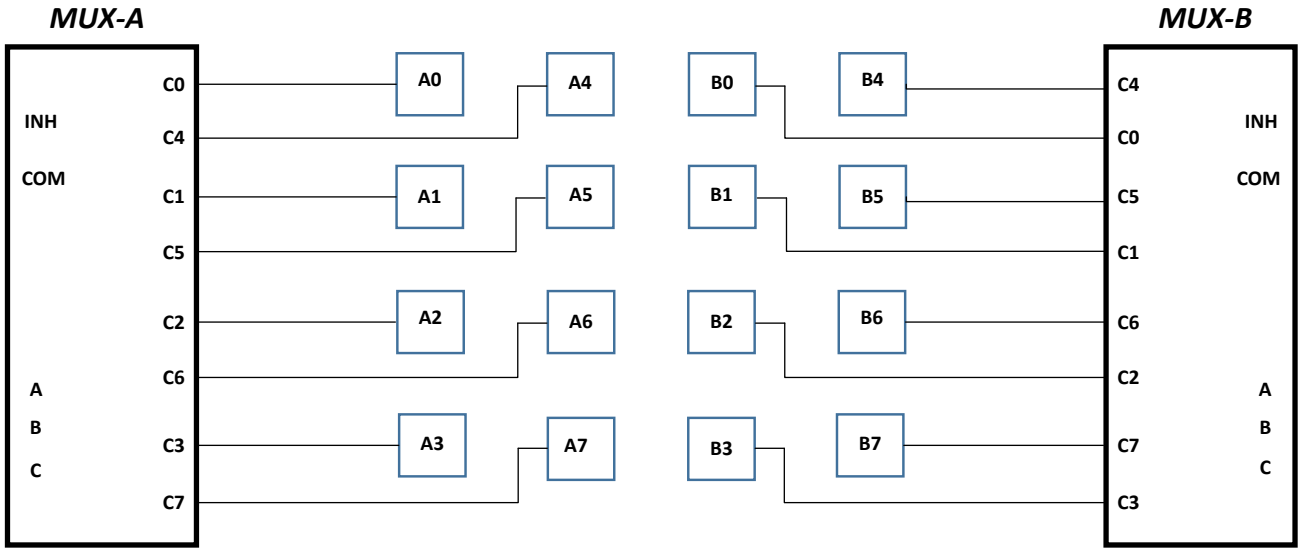

Figure 33. Schematic of the TSL235 matrix acquisition system

To acquire each TSL235 frequency value, it is necessary to select each one through the channels A, B and C, that are selector inputs. This selection is made by changing and combining the logic level of these selector inputs.

The result of this combination can be expressed as a truth table (Table 7).

The INH channel logic level must also be taken in account because when it is equal 1, all the IN/OUT Channels are disabled.

Table 7 – Channel Selection Truth Table [73]

INPUT STATES				**Channel IN/OUT Selected**
INHIBIT	**C**	**B**	**A**	
0	0	0	0	0
0	0	0	1	1
0	0	1	0	2
0	0	1	1	3
0	1	0	0	4
0	1	0	1	5
0	1	1	0	6
0	1	1	1	7
1	X	X	X	None

X – Don't care

These selector inputs and the INH channel will be controlled through a MCU. They will be connected to the MCU digital outputs, whose logic level variation will allow the acquisition of every TSL235 output value.

As the INH channels allow to disable all the IN/OUT channels, it is possible to control from which one of the CD4051Bs the data is acquired, allowing to interlink the channels A, B and C of MUX-A with the corresponding channels of MUX-B.

The acquisition of the TSL235 output values present on the IN/OUT channel selected is realized through the COM channels, that will be connected to the MCU input ports.

Since the TSL235 output is a frequency, it is necessary that the COM channels are connected to MCU inputs that allow frequency acquisition.

Therefore, is fundamental to choose a microcontroller that has, at least:

- Three digital outputs to communicate with the selection channels A, B and C;
- Two digital outputs to communicate with the INH channels of MUX-A and MUX-B;
- Two inputs able to acquire frequency values.

Figure 34 shows a schematic of the channel and port connections necessary between the two multiplexers CD4051B and a MCU.

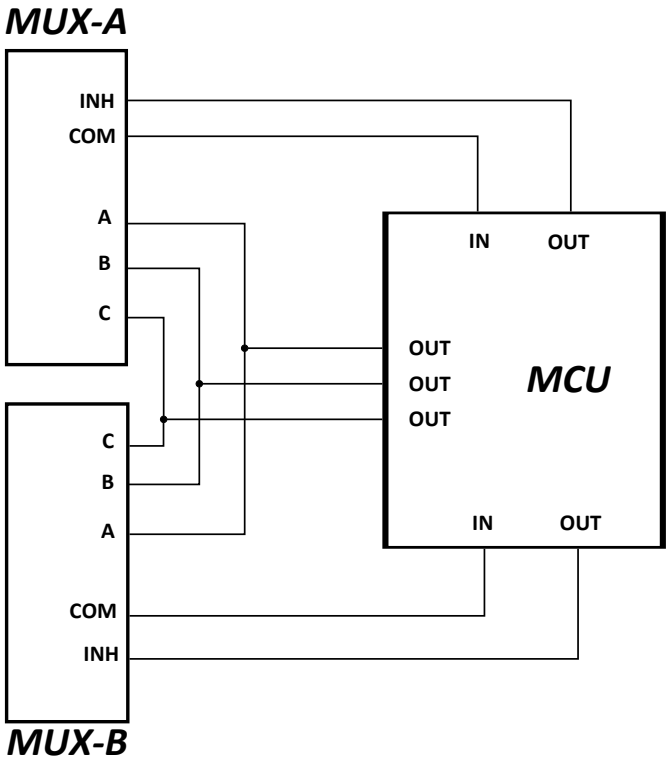

Figure 34. Schematic of the connection between MUX-A and MUX-B with a MCU

The Microcontroller selected to make the data acquisition, processing and communication is the 8-bits AVR ATmega328P by *Atmel*.

This MCU twenty-three general purpose I/O lines, internal and external interrupts, a maximum operating frequency equal 20 MHz, and operates between 1.8 and 5.5 volts [74].

Apart from these suitable technical characteristics, this MCU can be found already integrated in the development board Arduino Uno by *Arduino* (Figure 35), which aids in the elaboration of this work.

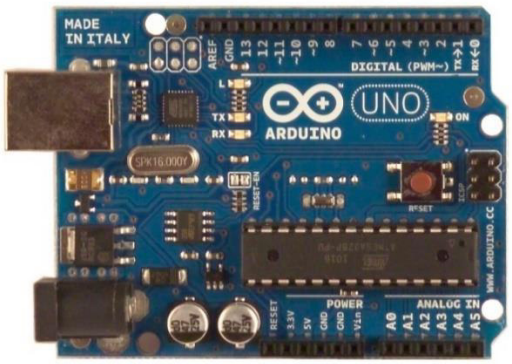

Figure 35. Microcontroller board Arduino Uno by Arduino [75]

The Arduino Uno main technical specifications are presented in Table 8.

Table 8 – Arduino Uno main technical specifications [75]

Microcontroller	ATmega328P *(Atmel)*
Operating Voltage	5 V
Input Voltage	Recommended: 7-12 V; Limit: 6-20 V
Digital IN/OUT Pins	14
PWM Digital IN/OUT Pins	6
Analog Input Pins	6
DC Current per IN/OUT Pin	20 mA
Clock Speed	16 MHz

The Arduino Uno board operates at 5 V, and can be powered via USB connection or with an external power supply. It has 14 digital and 6 analog pins. Each 14 digital pins used as an input or output, operate at 5 V and can provide or receive 20 mA (recommended). The 6 analog pins, labelled from A0 to A5, provide 10 bits of resolution and, by default, measure from ground to 5 V. Powering the Arduino Uno board via the USB connection also allows to interface with the computer through serial communication [75].

In addition to these specifications, there are some pins that have specialized functions [75]:

- Power:
    - Vin: input voltage to the Arduino board when using external power source;

- 5V: a 5 V supply;
- 3V3: a 3.3 V supply;
- GND: Ground;

- Serial Communication:
  - Digital Pin 0 (RX): used to receive (RX) Transistor-Transistor Logic (TTL) serial data;
  - Digital Pin 1 (TX): used to transmit (TX) TTL serial data;
- External Interrupts:
  - Digital Pins 2 and 3: can be configured to trigger and interrupt;
- PWM:
  - Digital Pins 3, 5, 6,9, 10 and 11: provide 8-bit PWM output;
- Serial Peripheral Interface (SPI):
  - Digital Pins 10 (SS), 11 (MOSI), 12 (MISO), 13 (SCK): support SPI communication;
- LED:
  - Digital Pin 13: built-in LED;
- Two Wire Interface (TWI):
  - Analog Pin 4 (SDA) and Analog Pin 5 (SCL): support TWI communication.

In Figure 36 is shown the MCU ATmega328P pin mapping, along with the Arduino functions corresponding to each pin.

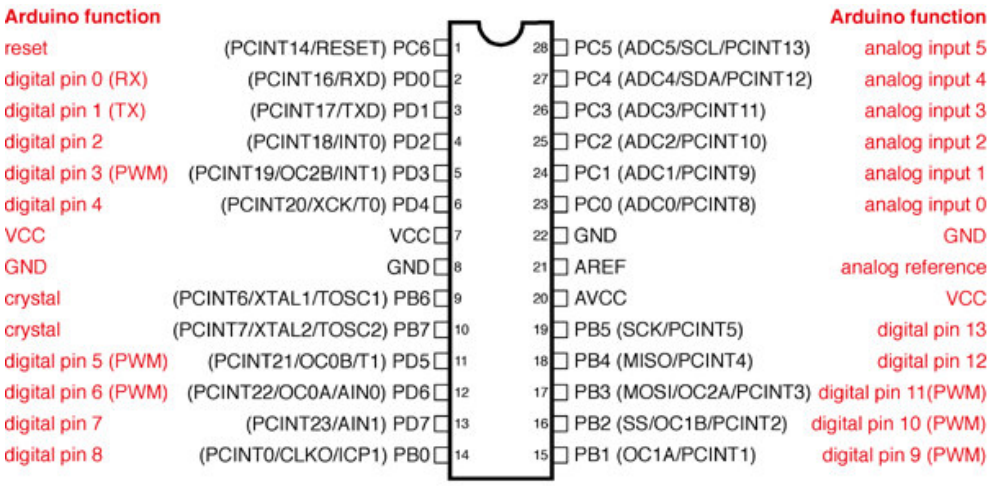

Figure 36. ATmega328P Pin Mapping and Arduino Functions [75]

It is critical to analyse the MCU ATmega328P and the Arduino Uno board and realise if their characteristics, specifications and function match with the other components and can fulfil the system requirements (Table 9).

Table 9 - Comparison between the Arduino Uno board and the system required specifications

	TSL235	**CD4051B**	**Arduino Uno**
Voltage	2.7 to 6.5 V	-0.5 to 20 V	Supplies 5 V
Current	3mA (max.)	-10 to 10 mA	Provides 20 mA (in each pin)
Ports		3 Ports - A, B and C	Digital Pins 8, 9 and 10
		2 Ports – 2 INH channels	Digital Pins 4 and 5
		2 Ports – 2 COM channels	Digital Pins 2 and 3 (External Interrupts)

Firstly, the Arduino Uno board operates at 5 volts, which goes in accordance with the operating voltage of the remaining components in the system: the TSL235 and the CD4051B operate between 2.7 and 6.5 V and between -0.5 and 20 V, respectively. This compatibility allows the Arduino Uno to be the power supplier to the other component, making the system power supply simpler. Each Arduino board digital pin can provide 20 mA at least, meeting the required supply current in the other components: -10 to 10 mA in the CD4051B and a maximum of 3mA in the TSL235.

To connect the Arduino Uno board with the remaining circuits, it is fundamental for it to have the required ports number and functions.

The A, B and C selection channels of the CD4051B have to be connect to digital pins since a logic level variation is needed. The Arduino Uno digital pins 8, 9 and 10 will be used for this function.

The INH channels will also have logic level variations, being necessary to connect them to digital pins as well. The two INH channels will be connected to the Arduino Uno digital pins 4 and 5.

The COM channels values will correspond to the measured frequency values. It is necessary to connect these channels to MCU pins able to read these types of values. The Arduino Uno presents

two digital pins (Digital Pins 2 and 3) with external interrupts, that can be configured to trigger an interrupt on a low value, a rising or falling edge, or a change of value [75]. This function will allow to receive and measure frequency values.

Figure 37 pictures a schematic of the interface circuit between the two CD4051B and the Arduino Uno board, with the representation of the connection between the multiplexers channels and the board pins.

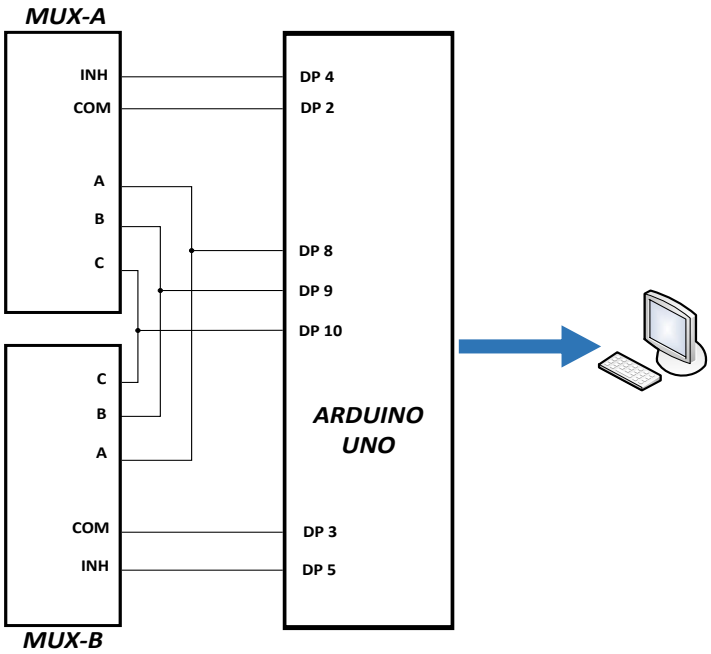

Figure 37. Schematic of the interface between the two multiplexers and the Arduino Uno

Figure X represents the schematic of the acquisition and communication systems, formed by the TSL235 matrix, the two CD4051B multiplexers and the MCU integrated in the Arduino Uno board.

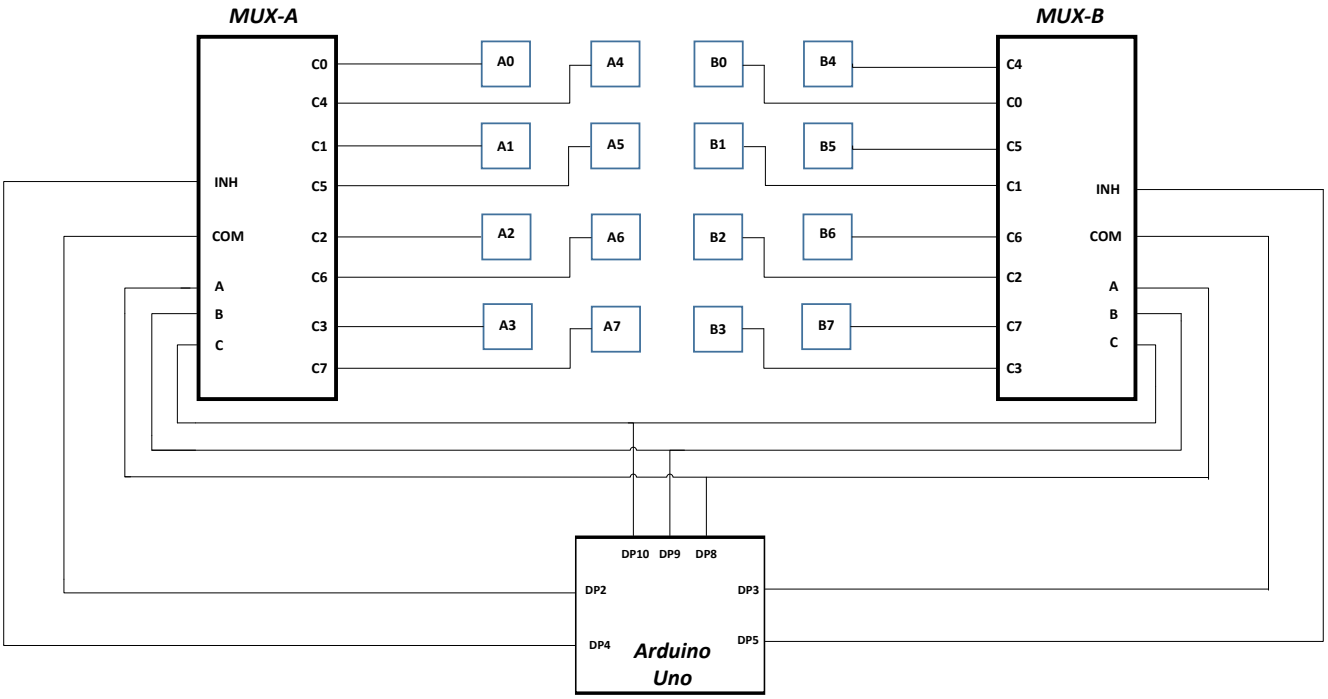

Figure 38. Schematic representation of the acquisition and communication systems.

After projecting all the fundamental circuits of this work, it is necessary to design and implement the whole system, considering all the package and pinout specifications.

4.3.2 Printed Circuit Board (PCB) design

To design and implement the detection system, a Printed Circuit Board (PCB) will be designed. A PCB design presents some advantages:

- Eliminates problems associated with the use of breadboards;
- Compact and optimized final product;
- Easy to replicate and change;

The circuit is going to be designed using the EAGLE software by *CadSoft Computer.* This software provides many important component libraries, like *Texas Instruments*, which is helpful to design a circuit with the correct layout.

Figure 39 and Figure 40 present the detection system schematic and board design in EAGLE.

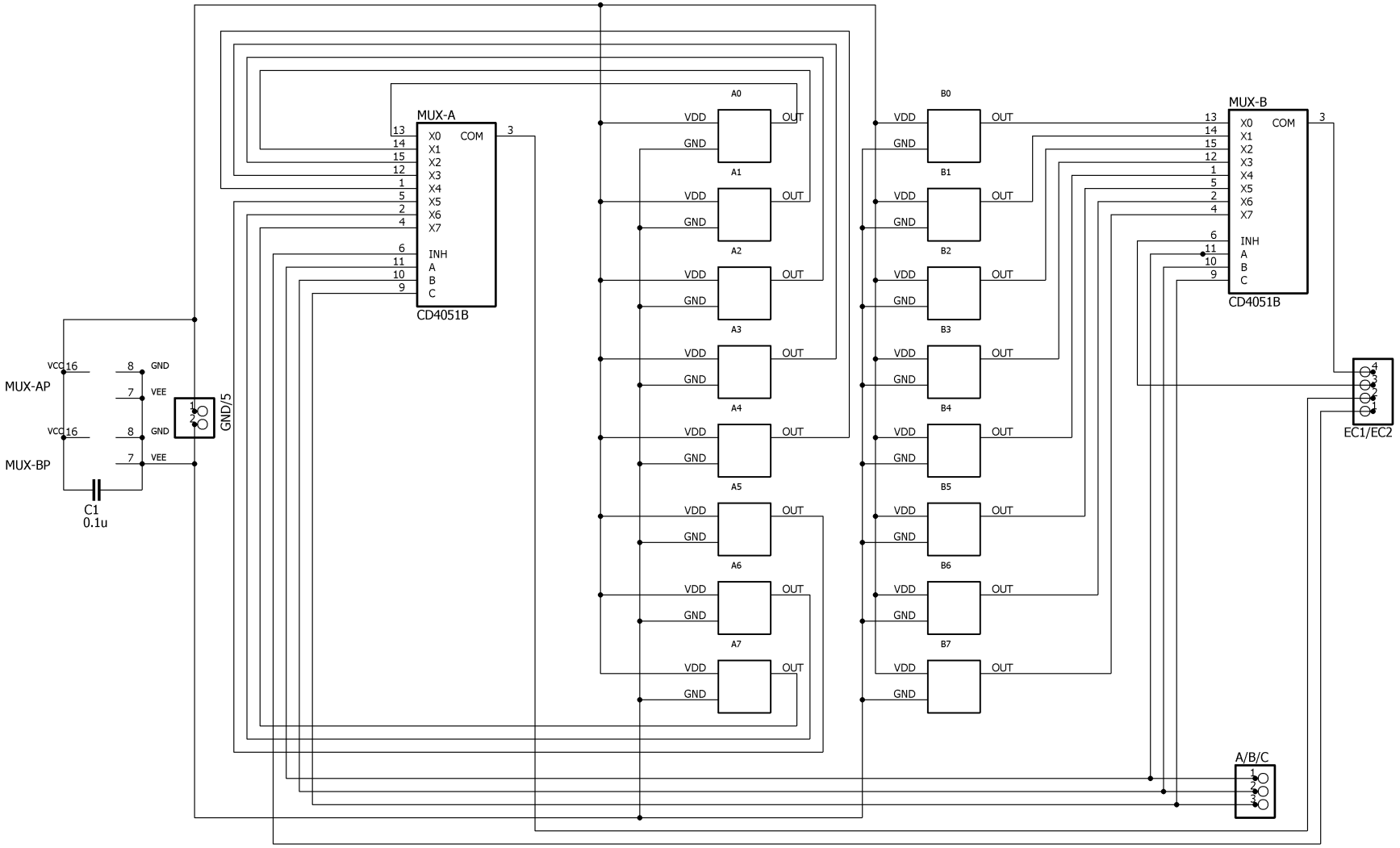

Figure 39. Detection system schematic design in EAGLE

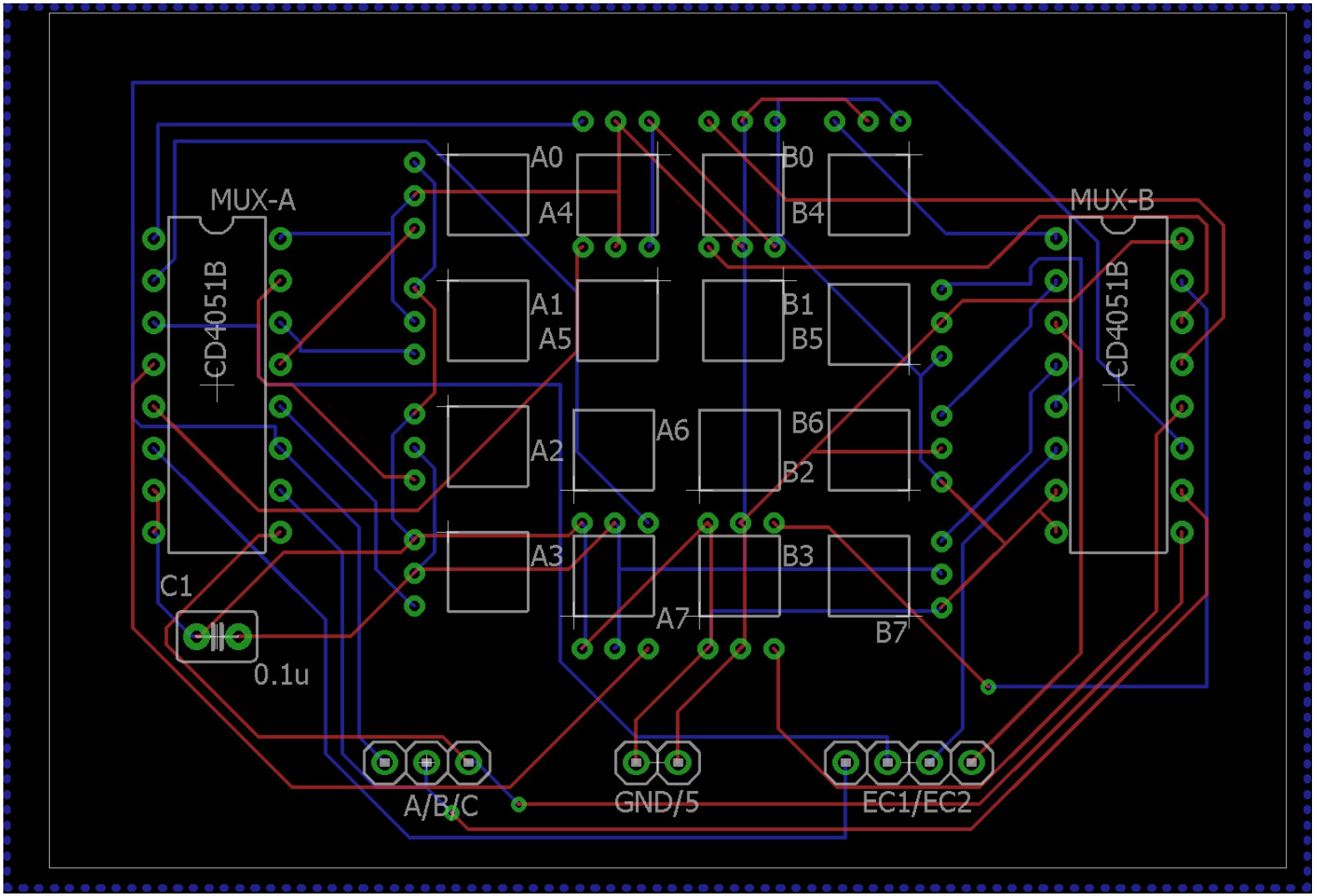

Figure 40. Detection system board layout design in EAGLE

In the board layout all the utilized components can be observed (TSL235 matrix, two CD4051B, a capacitor), and the headers to connect it to the Arduino Uno board.

The TSL235 matrix was designed considering factors like dimension and form. Its square form and significant dimension are present in Figure 41.

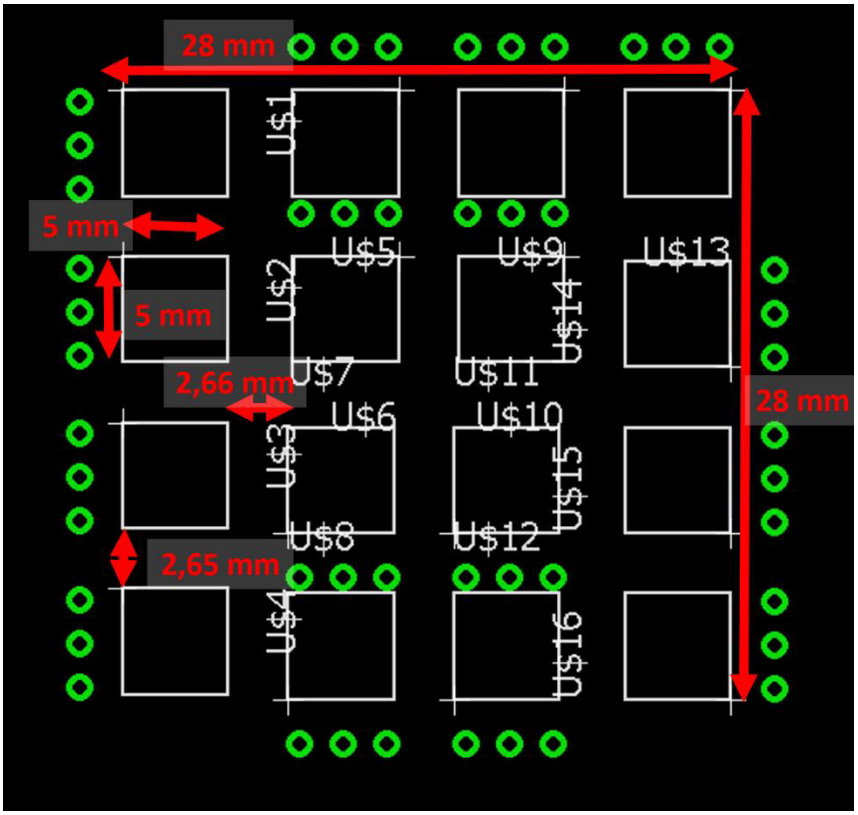

Figure 41. TSL235 matrix dimensions

The matrix presents 2.8 x 2.8 cm of dimension, forming a square. Analysing these characteristics, the sensors will be very close to each other, which leads to an adequate and compact form to perform its functions and carry out experimental tests in different environments and machines.

For a better visualization of the board designed, in Figure 42 a projection of the final product in 3D is presented, obtained from 3D BRD Viewer, a free tool developed by *Cytec BG* [76].

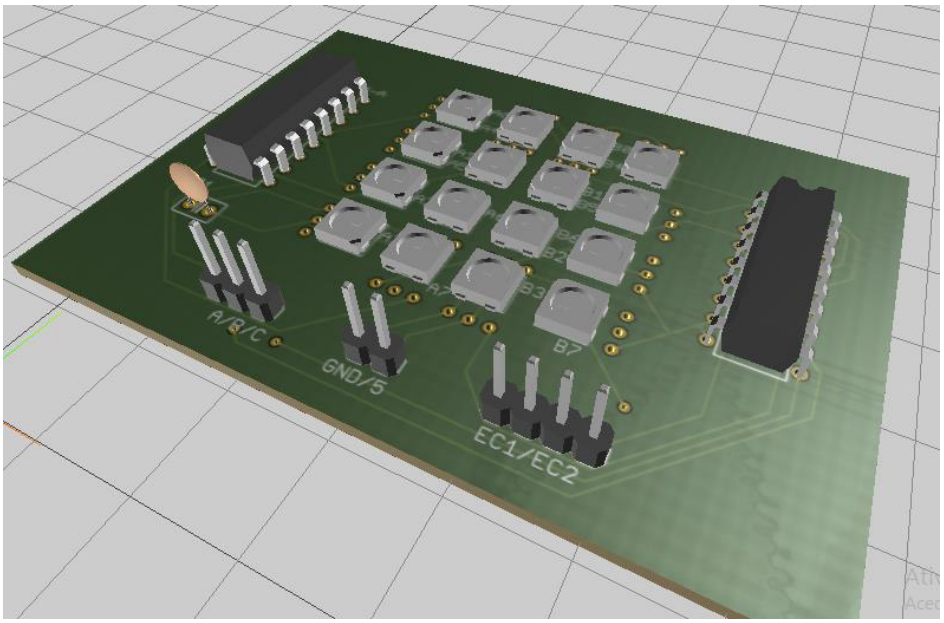

Figure 42. Detection system 3D image

4.3.3 Results

After projecting and designing the board, it is necessary to print and connect it to the MCU in order to test the whole system. Then it is necessary to assembly the components and connect them to the Arduino Uno board.

Figure 43 presents a photo of the board printed, before assembling the components.

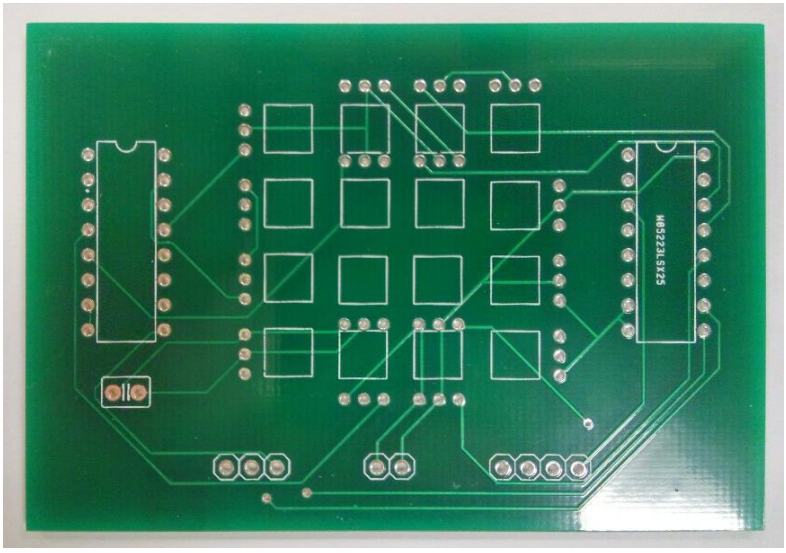

Figure 43. Photo of the PCB before assembling the components

After the components have been mounted, the final result of the board is presented in Figure 44.

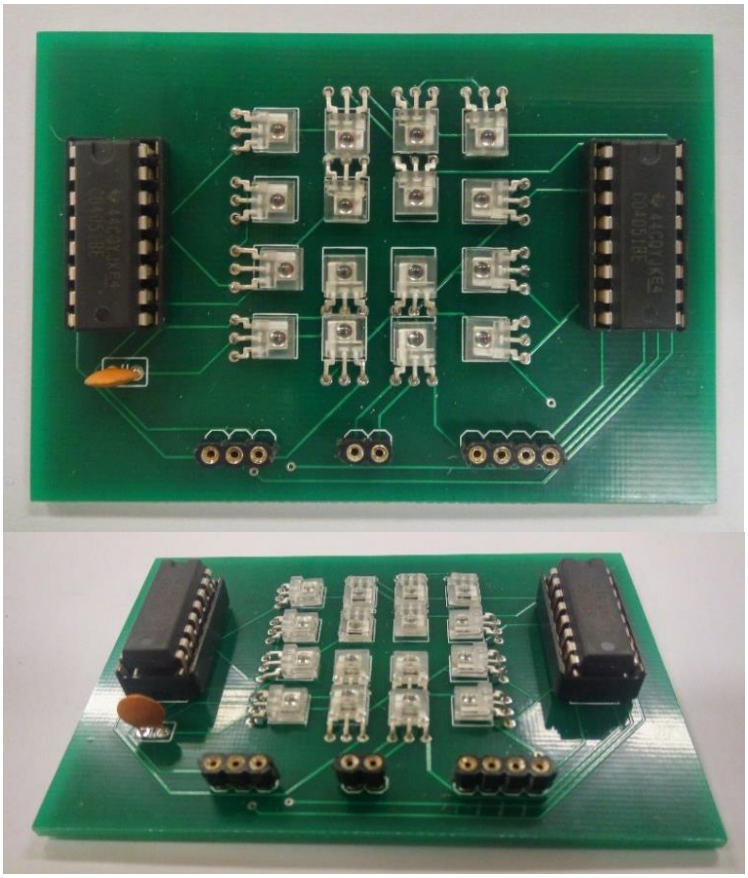

Figure 44. Final PCB assembled

The connection between the Detection board and the Arduino Uno is presented in Figure 45.

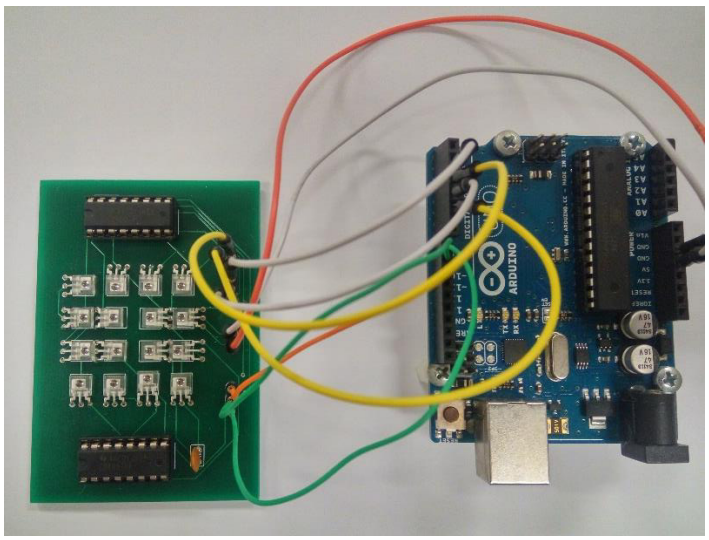

Figure 45. Connection between the Detection board and the Arduino Uno

Therefore, being all the connections corrected, the system is ready to be tested after the upload of the control firmware to the MCU.

4.4 Development of Firmware to the Microcontroller

The firmware of the MCU is the responsible for controlling all of the electronic system.
Every hardware present in the developed system is submitted to a steady and constant control that guarantees an adequate and synchronous operation of all components. This control is carried out by a MCU that fulfils all the communication requirements along with a trustful and solid firmware. A bug in the firmware can lead to some problems and errors, like incorrect sensor reading.

In this work, the firmware must have many functions:

- Control which multiplexer is active;
- Control which multiplexer channel is reading;
- Control the external interrupts;
- Acquire the sensors values.

Furthermore, the firmware has to be fluid and fast reading in order to prevent the acquisition of wrong or lagged values.

4.4.1 Software Analysis

To develop the firmware to control the detection system will be used the Arduino Integrated Development Environment – Arduino Software (IDE) by *Arduino* (Figure 46) [77].

Figure 46. Arduino Software (IDE) [77]

The Arduino Software (IDE) is a development platform dedicated to program and communicate with the Arduino hardware. It contains a text editor and a console and provides very comprehensive libraries with important functions already implemented allowing, at the same time, the development of code using C or C++ language (Figure 47).

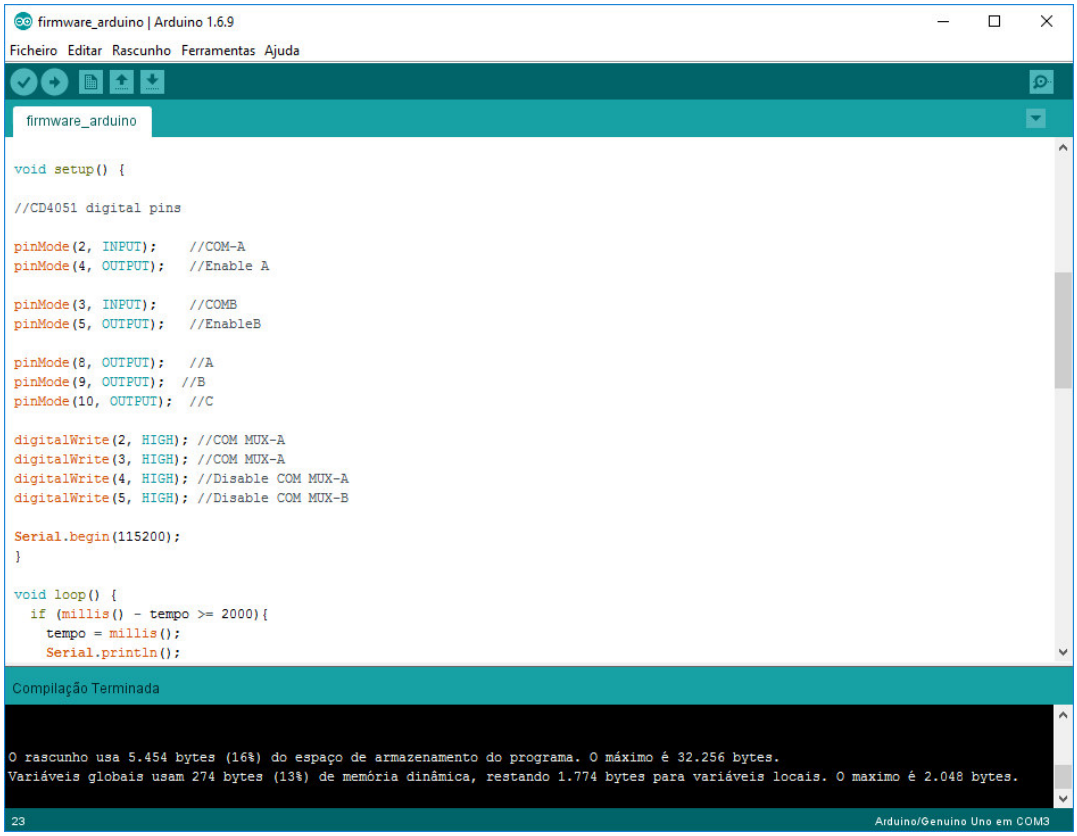

Figure 47. Arduino development platform

The platform also provides a Serial Monitor to display serial data sent from the Arduino board or send data to the board enabling a user-friendly interface.

4.4.2 Firmware Implementation

In view of the need to acquire valued from one TSL235 or from the matrix, it was developed a firmware to the MCU capable of handling both scenarios requiring only a few changes in the code.

The firmware has the ability to perform many functions:

- Enable and disable the multiplexers, controlling which is active and whence will be acquired the channel values;
- Select and control the acquisition of the channel values;
- Control the interrupts which may be useful in frequency values reading;
- Read, acquire and display the values at every time interval defined.

The flowchart represented in Figure 48 exposes, in a simplified way, the system control developed to the MCU.

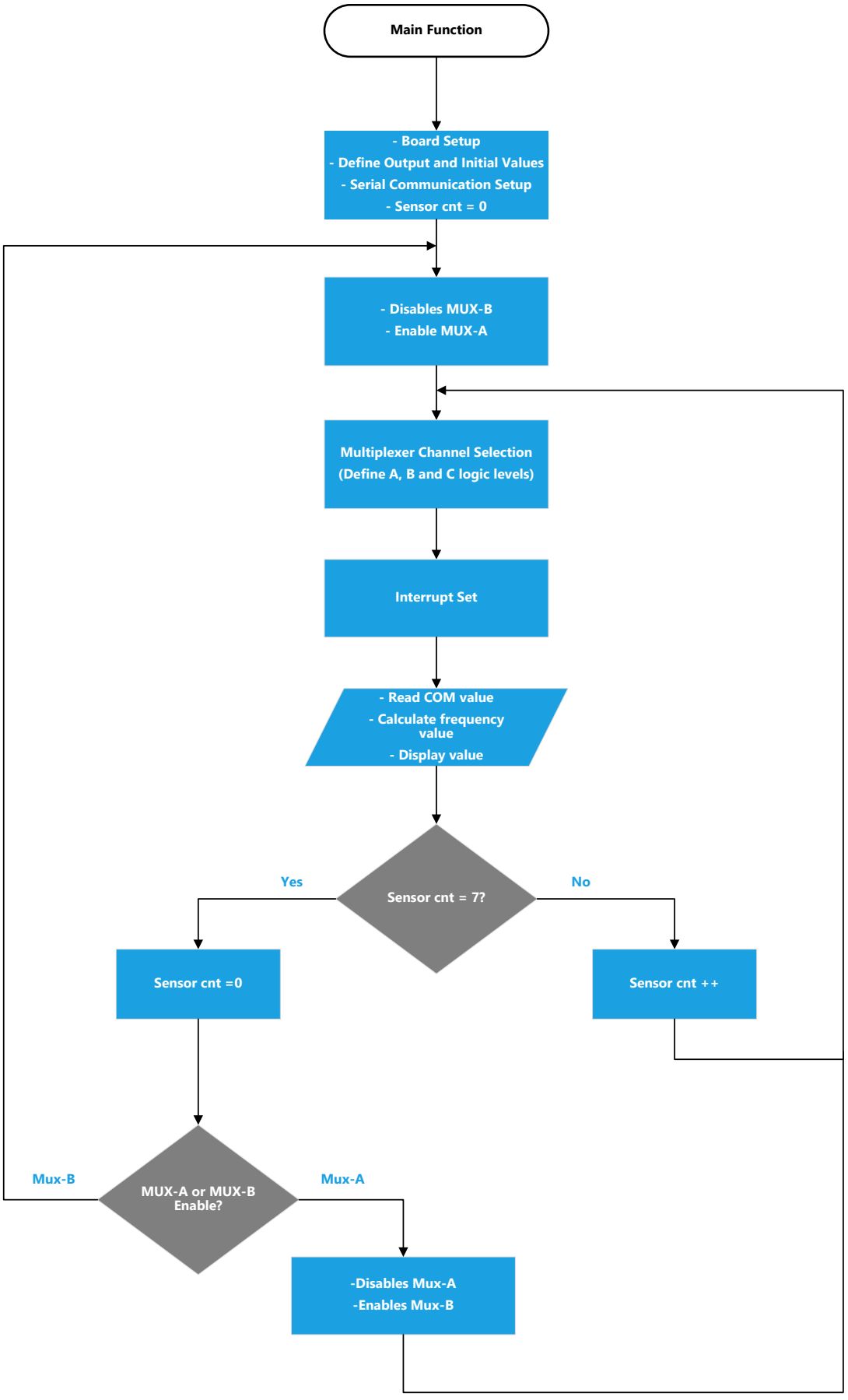

Figure 48. Flowchart representative of MCU Main Function

Initially the board configurations are setup, defining which are the input and output pins and its initial values. The firmware variables, such as variables to read the sensors values or to define A, B and C channels logic levels, are also defined and initialized, as is the sensor counter that will be used on the multiplexers channels selection.

Thereafter, the serial communication is configured, establishing conditions to the interface between the system and the computer.
The baudrate is configured at 115200 bits per second (bps) allowing a good data transfer rate.

The next step is to define which multiplexer will be active first, being the MUX-A enabled and MUX-B disabled at the first occurrence.
Then, the channel to read it is selected, defining the logic level of the output pins correspondents to the A, B and C MUX channels. The configuration of these channels is made in accordance with the truth table present in Table 7 and using the sensor counter. This counter defines which of channels is the selected one, changing the pins logic level through the *bitRead* function.
The *bitRead* function will read a desired bit of the counter value, matching the least-significant bit (LSB) with channel A, the middle bit with channel B and the most-significant bit (MSB) with channel C.

The external interrupt is set to allow the firmware to read the values present in the COM channels and calculate the related frequencies. The *attachinterrupt* function actives the interrupt, defines when it is triggered and which is the routine to call when it happens.
In this firmware, a mode is set to trigger the interrupt when the COM logic value goes from low to high level. This interrupt mode permits to count the number of pulses in the COM channel within a certain period of time using the routine called by the function.
Every time that the interrupt routine is called, a pulse counter is incremented. After a defined interval (for example, 50 milliseconds), the interrupt is disabled and the frequency is calculated using the following equation:

$$frequency = \frac{number\ of\ pulses}{time\ period} \quad (g)$$

Then, the frequency is displayed in the serial monitor and the pulse counter is reset.
Thereafter, it is verified if the channel read is the last of the active multiplexer. If it is not the last, the sensor counter is incremented and the A, B and C channels values are updated to acquire the values of the next sensor. If the channel read is the last, the sensor counter is reset and the active multiplexer is disabled. Then, the other MUX is enabled starting its sensors acquisition.

4.4.3 Results

Following the development of the code to the MCU, it is fundamental to test the functioning of the firmware along with the pre-selected hardware to verify if the whole detection system is operating properly.

While testing the system, it is noticed that the firmware implemented runs smoothly, controlling the pins correctly, selecting the sensors and multiplexers and acquiring the values as required.
The operating feedback is obtained continuously on the monitor through serial communication.
In Figure 49 an example of the user interface of the system through the Arduino Software serial monitor is shown.

The serial monitor presents all sixteen sensor values collected at each time interval defined (in this example, at each 2 seconds) in kHz. The values are divided into two groups, the MUX 1 and MUX 2, that correspond to MUX-A and MUX-B, respectively. This division is in accordance to Figure 31.

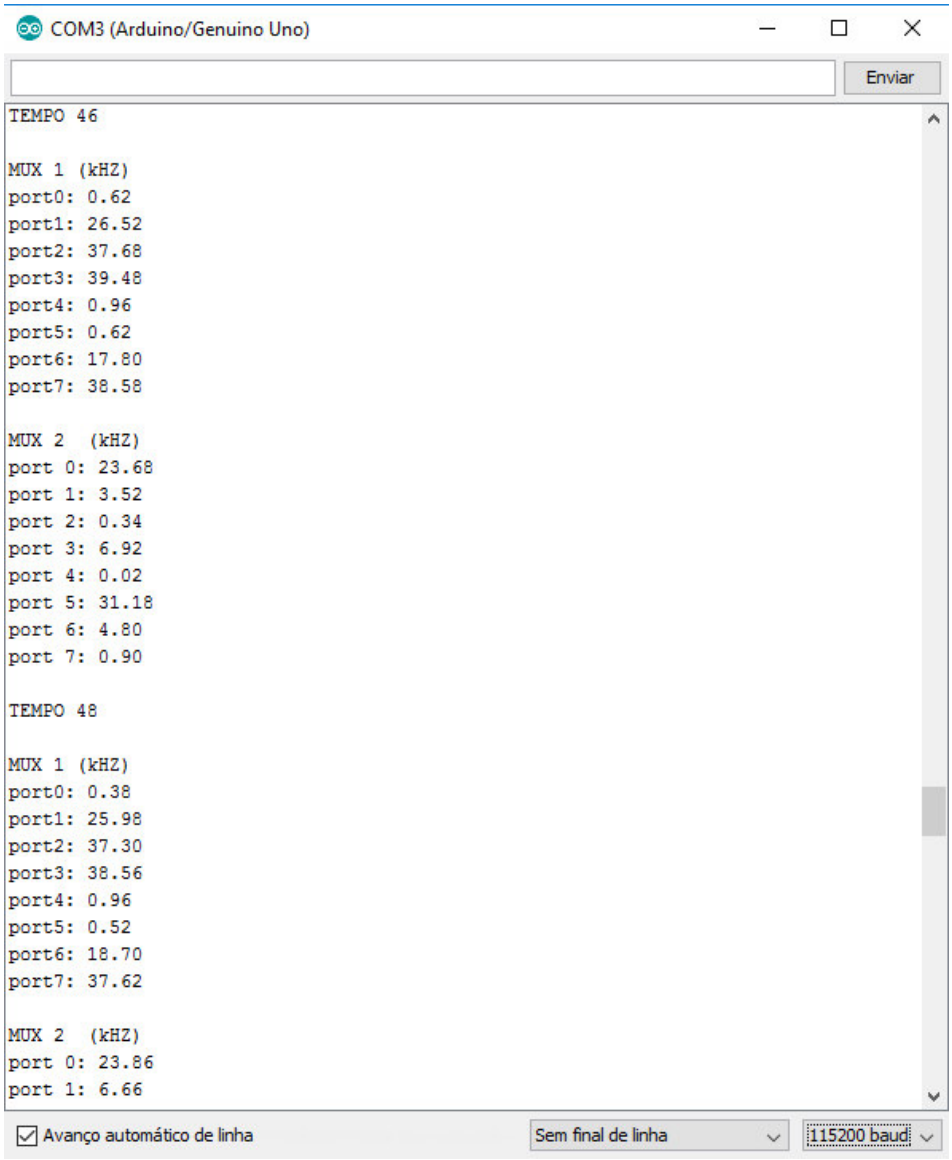

Figure 49. Results displayed on the Arduino Software serial monitor

The values obtained are ready to be analysed in order to verify and validate the conversion and acquisition results.

4.5 Conclusions

Figure 50 represents the block diagram of the system designed and implemented during the development of this work.

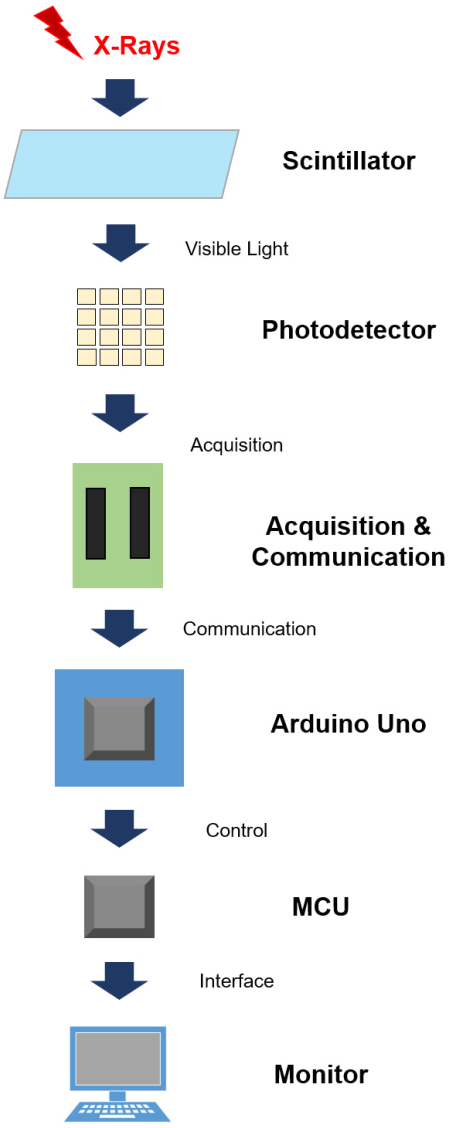

Figure 50. Developed system block diagram

Considering the results that were obtained and analysed previously, it can be concluded that the goals and requirements specified for this firmware were achieved.

A proper and secure control of the system hardware is presented, along with a solid and fluid firmware performance that is not susceptible to delays or crashes, and a constant value acquisition through serial communication.

The values processing and the results display through the serial monitor are also positive aspects of the firmware performance and the use of Arduino software in this work.

5. EXPERIMENTAL TESTS

5.1 Introduction

After the electronic circuits assembly and firmware implementation, it is necessary to test the performance of the whole system to acquire results from the X-rays into visible light conversion, in order to analyse and validate its operation.

This chapter covers the radiation source used, the methodology address in the experimental tests, and presents and analyses the results obtained from them.

5.2 Methodology

To perform the experimental tests and measurements a methodology was defined in order to analyse and validate the obtained results.
The method chosen to be applied to experimental tests is:

- Measurements without a Scintillator and Polymer-matrix film;
- Measurements with a pure Polymer-matrix;
- Measurements with the Polymer-based scintillator nanocomposites.

The polymer-matrix to be used is the SEBS, that may contain several scintillator nanocomposites (Gd_2O_3:Eu^{3+}) concentrations ranging from 0.25 to 0.75 wt.%.

It is necessary to run different tests with a pure SEBS and a SEBS with scintillating nanocomposites samples to validate if the X-rays to visible light conversion is happening and if its results are satisfactory.

To test the system, an X-ray beam will fall on the sensor or sensors. This beam will suffer an increasing power variation due to the induced current increase. The beam power range is defined according to the radiation source and its characteristics.

The radiation source output beam is powered with a voltage of 40 kV and a current ranging from 0 to 40 mA, which leads to an output power ranging from 400 to 1600W (Table 10).

Table 10. Output X-rays Beam Power Range

Voltage, V (kV)	**Current, I (mA)**	**Power, P: V*I (W)**
40	0	0
	10	400
	20	800
	40	1200
	40	1600

The sensor values were collected for each beam power value in order to make a characterization of the system.

In this process it is expected an increasing progression of the collected results as the beam power increases since the visible light generated intensity is directly proportional to the incident beam power, thereby increasing proportionally the frequency measured [4].

5.3 Results

5.3.1 Single Sensor & Scintillator Characterization

Experimental tests were performed to measure and evaluate the X-rays into visible light conversion by Gd_2O_3:Eu^{3+}/PPO/POPOP/SEBS composite films, with nanoparticles content ranging from 0 to 0.75 wt.%, with just one TSL235 photodetector.

These experiments took place using the radiation source Bruker D8 Discover diffractometer [78]. This source allows the emission of an X-ray beam with several electric power values, which is very important to characterize and analyse the system operation.

To carry out the measurements and test, a scintillator sample was placed above the sensor subject to the radiation beam incidence.

The disadvantage of using this radiation source is the short area of the emitted beam, making it impossible to be detected by many sensors at the same time, allowing measurements with only one sensor.

Figure 51 shows the visible radiation intensity (V.R.I) as a function of the X-ray output power.

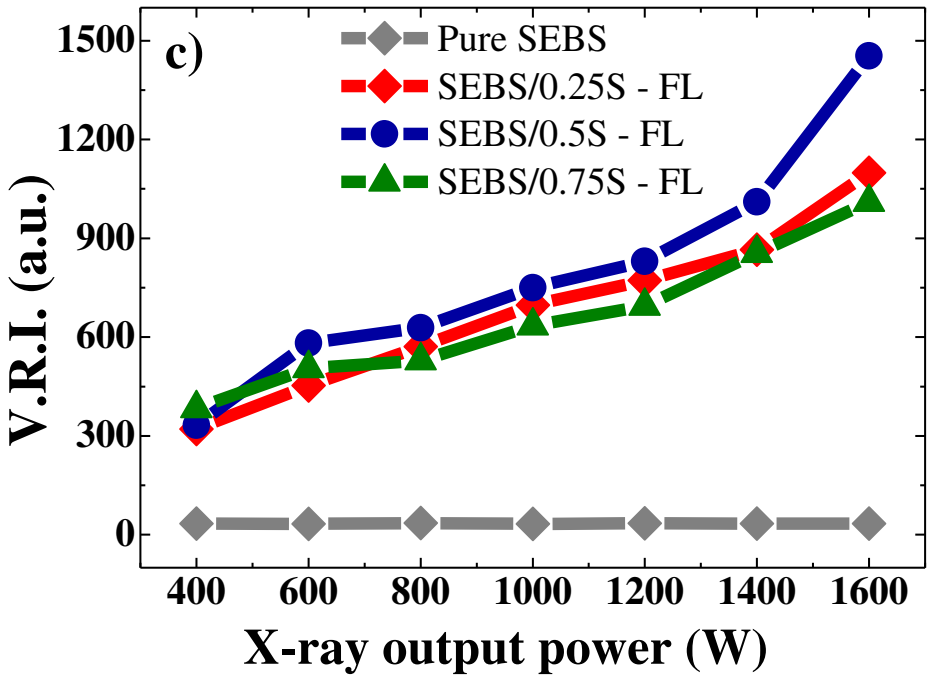

Figure 51. Variation of the visible radiation intensity (V.R.I) as a function of the X-ray output power (W)

The results obtained show a proportional increase of the converted light intensity regarding the X-ray output power increase, which supports the expectations described above [4]. It can also be observed that higher scintillator nanoparticles content leads to a higher visible light generation rate. However, after a certain scintillator filler content, the visible radiation detection may decrease due to higher light dispersion and decreased optical transparency of the films.

Figure 52 shows the variation of V.R.I. as a function of $Gd_2O_3:Eu^{3+}$ content, with and without the inclusion of the fluorescence molecules.

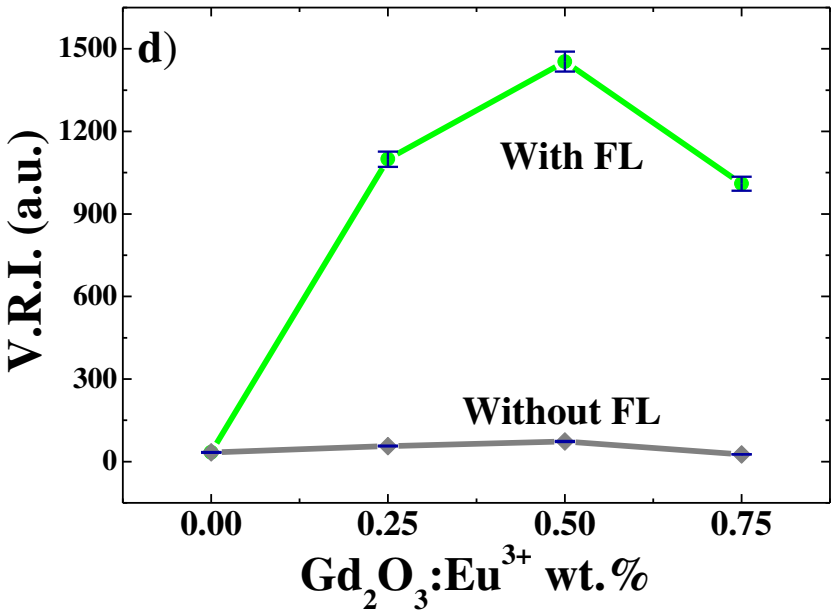

Figure 52. Variation of the visible radiation intensity as a function of $Gd_2O_3:Eu^{3+}$ content (wt %), with and without fluorescence molecules

The inclusion of low contents of fluorescence molecules on the scintillator process improves composite scintillator performance, confirming this approach to be a suitable solution for improving the performance of polymer-based composites for X-ray detection.

5.3.2 Matrix Sensors Characterization

To verify the operation of the TSL235 matrix, singular experimental tests were performed to its sensors.

However, due to the radiation source space and design limitations, it was only possible to measure and acquire the sensors values from the first row of the matrix (Figure 53). From these four sensors, one from the centre and one from the edge were selected.

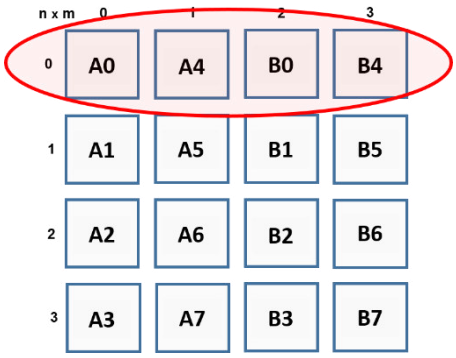

Figure 53. Sensors from the first row of the matrix

In order to check the operation of the two multiplexers, one sensor from each MUX were selected. Therefore, the sensors tested were the sensor A0 and B0.

Figure 54 presents the system board placed on the radiation source, ready to be tested.

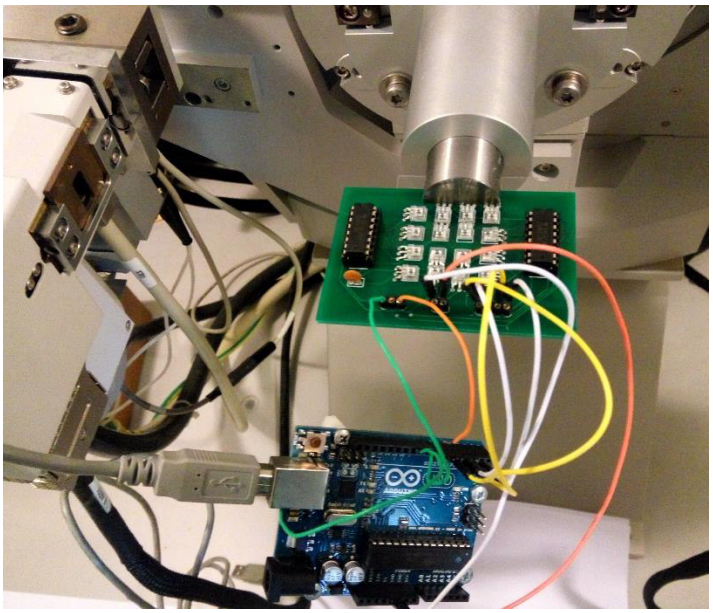

Figure 54. Photo of the system board and Arduino placed on the radiation source

In these experiments, the experimental methodology defined previously was followed, with the particularity that only the Gd_2O_3:Eu^{3+}/PPO/POPOP/SEBS composite film with 0.50 wt.% nanoparticles content was picked, due to its better and suitable results on the previous characterization (Figure 51 and Figure 52).

Figure 55 shows the visible radiation intensity (V.R.I.) acquired from the sensor A0 as a function of the X-ray output power.

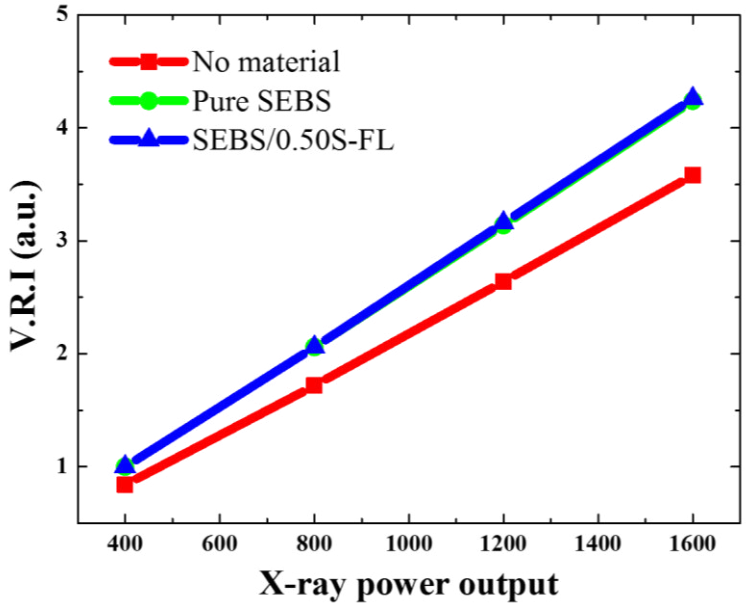

Figure 55. Visible Radiation Intensity measured on sensor A0

Figure 56 is a representation of the V.R.I. measured from the sensor B0 as a function of the X-ray output power.

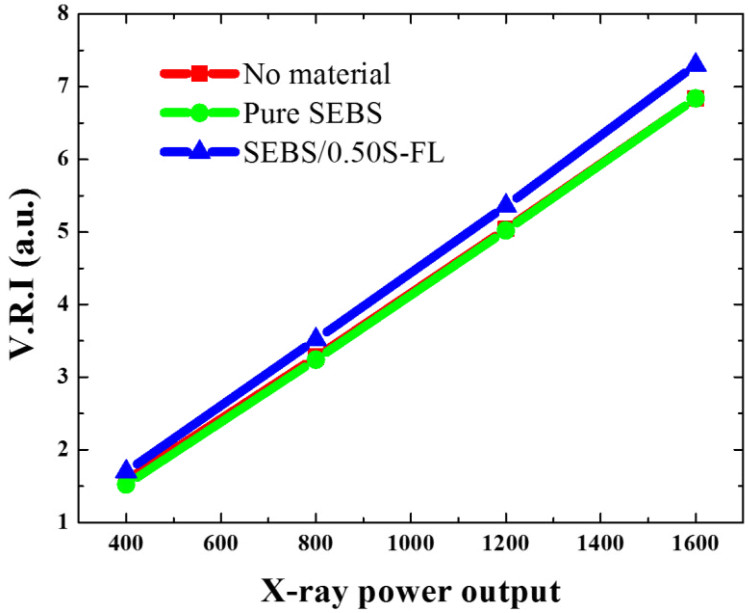

Figure 56. Visible Radiation Intensity measured on sensor B0

These characterizations and experimental tests followed the methodology defined previously, with the X-ray beam power being increased from 400 to 1600 W. The X-ray output power increase results in an increasing visible radiation intensity, that was acquired in kHz, in both sensors.

Although the experimental results are acceptable, the experimental conditions have to be improved in order to obtain optimized results since it is not to be expected an increasing output from the sensors with no scintillator particles. Even so, the sensors with the SEBS/0.50S-FL collected, as expected, the best results.

5.3.3 System Characterization

The whole system (detection system and the scintillator material) was subjected to experimental tests in order to verify and validate its performance.

In these experiments the radiation source used was a RX EVO-F by *Fujifilm*, a complete X-ray room solution which supports a comprehensive range of examinations [79]. This X-ray solution allows to test the system without area and space limitations and can acquire its own radiographs, which is an interesting feature to verify the scintillation materials performance (Figure 57).

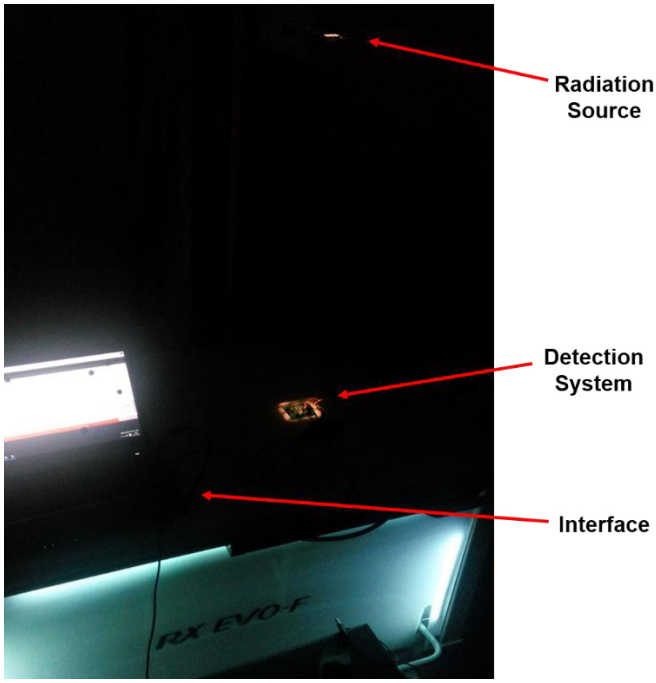

Figure 57. Radiation Source RX EVO-F by Fujifilm

During these experiments, the matrix values acquisition and the radiographs capture occurred simultaneously, in order to save resources and energy.

As in the previous test, only the composite film with 0.50 wt.% scintillator nanoparticles content was selected.

Figure 58 presents the system already connected and ready to be submitted to the tests.

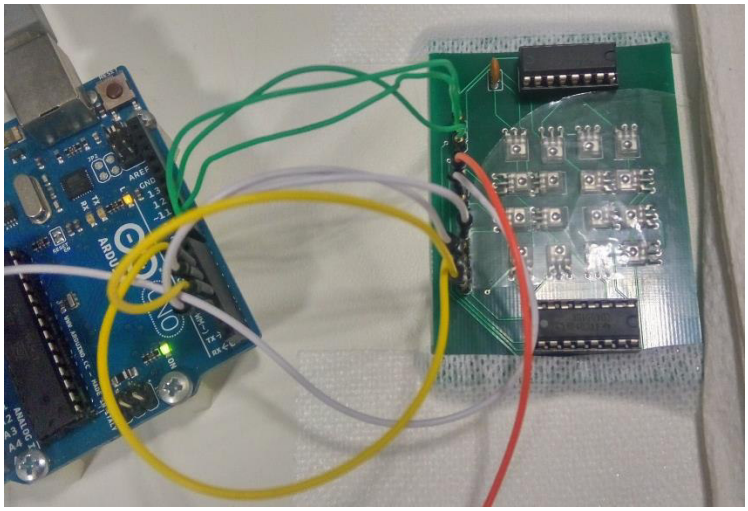

Figure 58. Photo of the system ready to be tested

Figure 59 presents the result of the three radiographs capture. In order to help on the analysis of these radiographs, an orange was placed on the top of the system. Due to its different compositions (peel, segments, seeds and juice) and densities, an orange is already used in several X-ray tests.

Figure 59 a) and Figure 59 b) are the radiographs of the set without any material and with a pure SEBS film on top of the sensors matrix, respectively.

Figure 59 c) presents the radiograph of the set "system + orange" with a SEBS/0.5wt.% film on top of the matrix.

Analysing and comparing the radiographs obtained, one can note a contrast similarity between Figure 59 a) and b). This similarity of contrasts is expected since none of the systems had a scintillator material. On the other hand, Figure 59 c) presents much more brightness due to the inclusion of the scintillator nanoparticles on the SEBS film since these particles also convert X-rays into visible light.

a) Radiograph without material

b) Radiograph with pure SEBS film

c) Radiograph with SEBS/0.50S-FL

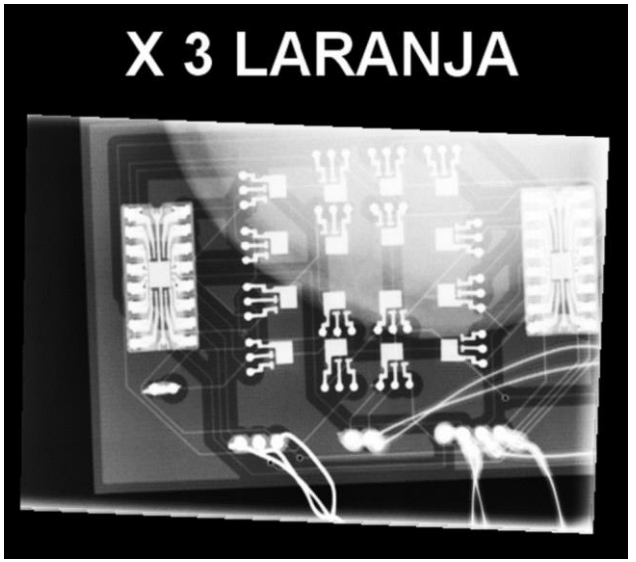

Figure 59. Radiographs resultant from the experimental tests. a) Radiograph without any material; b) Radiograph with a Pure SEBS film; c) Radiograph with a SEBS/0.5S.FL film

These results help to validate the performance of the scintillator material since considerable difference is observed between the brightness of the first two images and the third.

However, the values acquired from the detection matrix during the experiments did not meet the expectations. Despite detecting the room's visible light, the system did not obtain the expected results from the X-ray conversion by the scintillator material. This setback may result of several factors such as a higher output light dispersion, due to the higher conversion area, or a possible interference of X-ray beams with the remaining electronic components and the PCB.

Given the impossibility of repeating these experiments using the same radiation source, these have to be realized again in future work, identifying which problem, mentioned or not, has to be solved or if it is necessary to adopt new approaches or methodologies.

5.4 Conclusions

The developed system throughout this work was meant to integrate an innovative, flexible and low cost scintillator material with a light detection circuit able of acquiring the results from the conversion performed by the scintillator. This system had to clearly obtain and process the data, send it through serial communication, and present it to the user.

Based on the results obtained, one considers that the integration between the scintillator material and the detection circuit was well designed and implemented.
The data acquisition, communication and interface meet the intended requirements. However, since the results measured in the last experiments did not have the expected values, it is necessary to analyse and solve possible problems or adopt different experimental approaches/methodologies.

Still, the system presents the result clearly, dividing the values by multiplexer and by sensor while its user-friendly implementation allows a partial or complete modification of the program to implement the desired conditions for data acquisition.

6. CONCLUSIONS AND FUTURE WORK

In this chapter a final conclusion is presented, based on what was developed and analysed throughout this work. Some corrections, improvements and new approaches are also suggested, as they should be taken into account in future research.

Once all the steps to develop an X-ray detection system based on scintillator composites are completed, it is necessary to analyse the process and its results with more detail.

First, a polymer-based scintillator composite capable of join scintillating properties, converting radiation into visible light was prepared, with innovative characteristic like flexibility, stretchability and low cost. This scintillator material allows the development of effective radiation detectors for large areas and new applications. However, it is fundamental to do a more objective characterization of its properties in order to be correctly adapted to each application.

Thereafter a system able to detect and acquire the X-rays converted into visible light by the scintillator composite was developed. It was selected a sensor that measures the visible light and converts it into an electric signal. In addition to a single sensor circuit, a detection matrix to verify and validate the possibility of a large detection area based on scintillator composites was designed and implemented. To develop this matrix, the implementation of a circuit capable of obtaining all the matrix values, process and send them through serial communication to a user-interface was necessary. Both detection circuit and acquisition/communication circuit present a very satisfactory integration and performance, executing in an appropriate and solid way.

Finally, a firmware for the microcontroller was developed so to control the system acquisition and communication, as well as clearly display the results to the user.

With the realized experiments one can observe that the system presents great performance, both in X-ray conversion by the scintillator composites and the results acquisition and display. Also, its compact dimensions, good integration and low cost allow its utilization in new applications across many fields. However, the results obtained in the last test did not meet the expectations, which

leads to consider the system's problems/limitations along with possible solutions, and adopting other approaches and/or methodologies.

In a future work, for the improvement of the system, a light detection circuit based in printed photodetection matrices should be developed. The development of this system will allow its total integration and flexibility, making it capable of being reproduced in large area and scale and allowing its utilization in completely innovative applications.

In essence, the system meets the requirements and work objectives, being capable to acquire, convert, measure and display the X-ray detection values.
For a future work, it is necessary to optimize and solve the system problems and limitations, as well as to develop a detection circuit based on printed photodetection matrices.

BIBLIOGRAPHY

[1] J. G. Rocha, G. Minas, and S. Lanceros-Méndez, "Pixel readout circuit for X-ray imagers," 2010.

[2] J. G. Rocha, R. A. Dias, L. M. Gonçalves, G. Minas, A. Ferreira, C. M. Costa*, et al.*, "X-Ray image detector based on light guides and scintillators," 2009.

[3] J. G. Rocha, L. M. Goncalves, and S. Lanceros-Mendez, "Flexible x-ray detector based on the seebeck effect," in *2007 IEEE International Symposium on Industrial Electronics*, 2007, pp. 1525-1529.

[4] P. M. Martins, P. M. Martins, V. Correia, J. G. Rocha, and S. Lanceros-Mendez, "Gd2O3: Eu nanoparticle-based poly (vinylidene fluoride) composites for indirect X-ray detection," *Journal of Electronic Materials,* vol. 44, pp. 129-135, 2015.

[5] J. Oliveira, P. M. Martins, P. L. A. Martins, V. Correia, J. G. Rocha, and S. Lanceros-Méndez, "Gd2O3: Eu3+/PPO/POPOP/PS composites for digital imaging radiation detectors," 2015.

[6] C. Blakemore and S. Jennett, *The Oxford Companion to The Body*: Oxford University Press, 2001.

[7] G. Blasse and B. Grabmaier, *Luminescent materials*: Springer Science & Business Media, 2012.

[8] W. C. Röntgen, "On a New Kind of Rays," *The British Journal of Radiology,* vol. 4, pp. 32-33, 1931.

[9] Deutsches Röntgen-Museum. (May 2016). Available: http://www.roentgen-museum.de/

[10] i3system Inc. (September 2016). *Digital X-Ray*. Available: http://www.i3system.com/

[11] J. Selman, *The Fundamentals of X-Ray and Radium Physics*: Literary Licensing, LLC, 2012.

[12] M. Korner, C. H. Weber, S. Wirth, K.-J. Pfeifer, M. F. Reiser, and M. Treitl, "Advances in Digital Radiography: Physical Principles and System Overview 1," *Radiographics,* vol. 27, pp. 675-686, 2007.

[13] J. Als-Nielsen and D. McMorrow, *Elements of modern X-ray physics*: John Wiley & Sons, 2011.

[14] R. L. Smathers and W. R. Brody, "Digital radiography: current and future trends," *The British journal of radiology,* vol. 58, pp. 285-307, 1985.

[15] J. Silva, S. Lanceros-Mendez, G. Minas, and J. G. Rocha, "CMOS X-ray image sensor array," in *Electronics, Circuits and Systems, 2007. ICECS 2007. 14th IEEE International Conference on*, 2007, pp. 1067-1070.

[16] J. G. Rocha, L. M. Goncalves, and S. Lanceros-Mendez, "Bi2Te3-Sb2Te3 on polymeric substrate for X-ray detectors based on the seebeck effect," *Microsystem Technologies,* vol. 18, pp. 1-8, 2012.

[17] G. F. Knoll, *Radiation detection and measurement*: John Wiley & Sons, 2010.

[18] C. W. van Eijk, "Inorganic scintillators in medical imaging detectors," *Nuclear Instruments and Methods in Physics Research Section A: Accelerators, Spectrometers, Detectors and Associated Equipment,* vol. 509, pp. 17-25, 2003.

[19] G. Blasse, "Luminescent materials: Is there still news?," *Journal of Alloys and Compounds,* vol. 225, pp. 529-533, 1995.

[20] S. C. Curran, *Luminescence and the scintillation counter / by S.C. Curran*. London: Butterworths Scientific, 1953.

[21] G. Blasse, "Scintillator materials," *Chemistry of Materials,* vol. 6, pp. 1465-1475, 1994.

[22] P. A. Rodnyi, *Physical Processes in Inorganic Scintillators*: Taylor & Francis, 1997.

[23] C. R. Ronda, *Luminescence: from theory to applications*: John Wiley & Sons, 2007.

[24] J. Lilley, *Nuclear physics: principles and applications*: John Wiley & Sons, 2013.

[25] J. G. Rocha, "Microdetectores de silício baseados em cintiladores para radiografia digital," Departamento de Eletrónica Industrial, Universidade do Minho, 2003.

[26] E. V. van Loef and K. S. Shah, "Advances in scintillators for medical imaging applications," 2014, pp. 92140A-92140A-5.

[27] B. D. Milbrath, A. J. Peurrung, M. Bliss, and W. J. Weber, "Radiation detector materials: An overview," *Journal of Materials Research,* vol. 23, pp. 2561-2581, 2008.

[28] W. Cai, Q. Chen, N. Cherepy, A. Dooraghi, D. Kishpaugh, A. Chatziioannou*, et al.*, "Synthesis of bulk-size transparent gadolinium oxide–polymer nanocomposites for gamma ray spectroscopy," *Journal of Materials Chemistry C,* vol. 1, pp. 1970-1976, 2013.

[29] Y. S. Zhao, H. Zhong, and Q. Pei, "Fluorescence resonance energy transfer in conjugated polymer composites for radiation detection," *Physical Chemistry Chemical Physics,* vol. 10, pp. 1848-1851, 2008.

[30] W. Obitayo and T. Liu, "A Review: Carbon Nanotube-Based Piezoresistive Strain Sensors," *Journal of Sensors,* vol. 2012, p. 15, 2012.

[31] M. C. Righetti, A. Boggioni, M. Laus, D. Antonioli, K. Sparnacci, and L. Boarino, "Thermal and mechanical properties of PES/PTFE composites and nanocomposites," *Journal of Applied Polymer Science,* vol. 130, pp. 3624-3633, 2013.

[32] A. Quaranta, S. M. Carturan, T. Marchi, V. L. Kravchuk, F. Gramegna, G. Maggioni*, et al.*, "Optical and scintillation properties of polydimethyl-diphenylsiloxane based organic scintillators," *IEEE Transactions on Nuclear Science,* vol. 57, pp. 891-900, 2010.

[33] V. Milinchuk, N. Bolbit, E. Klinshpont, V. Tupikov, G. Zhdanov, S. Taraban*, et al.*, "Radiation-induced chemical processes in polystyrene scintillators," *Nuclear Instruments and Methods in Physics Research Section B: Beam Interactions with Materials and Atoms,* vol. 151, pp. 457-461, 1999.

[34] B. A. Gorelik and M. B. Voskobojnik, "Flexible highly filled coatings based on PVDF," *Journal of Fluorine Chemistry,* vol. 104, pp. 73-77, 6// 2000.

[35] N. A. Peppas and E. W. Merrill, "Development of semicrystalline poly (vinyl alcohol) hydrogels for biomedical applications," *Journal of Biomedical Materials Research,* vol. 11, pp. 423-434, 1977.

[36] S. Ribeiro, P. Costa, C. Ribeiro, V. Sencadas, G. Botelho, and S. Lanceros-Méndez, "Electrospun styrene–butadiene–styrene elastomer copolymers for tissue engineering applications: Effect of butadiene/styrene ratio, block structure, hydrogenation and carbon nanotube loading on physical properties and cytotoxicity," *Composites Part B: Engineering,* vol. 67, pp. 30-38, 12// 2014.

[37] J. G. Rocha and S. Lanceros-Méndez, "Review on X-ray detectors based on scintillators and CMOS technology," 2011.

[38] T. Sakellaris, G. Spyrou, G. Tzanakos, and G. Panayiotakis, "Monte Carlo simulation of primary electron production inside an a-selenium detector for x-ray mammography: physics," *Phys Med Biol,* vol. 50, pp. 3717-38, Aug 21 2005.

[39] J. G. Rocha and S. Lanceros-Mendez, "X-ray imaging matrix with light guides and intelligent pixel sensors, radiation or high energy particle detector devices that contain it, its fabrication process and its use," ed: Google Patents, 2008.

[40] P. Kleimann, J. Linnros, C. Frojdh, and C. S. Petersson, "An X-ray imaging pixel detector based on a scintillating guides screen," in *Nuclear Science Symposium, 1999. Conference Record. 1999 IEEE*, 1999, pp. 222-225.

[41] J. G. Rocha and S. Lanceros-Mendez, "3-D modeling of scintillator-based X-ray detectors," *IEEE Sensors Journal,* vol. 6, pp. 1236-1242, 2006.

[42] E. Hecht, "Optics 2nd edition," *Optics 2nd edition by Eugene Hecht Reading, MA: Addison-Wesley Publishing Company, 1987,* vol. 1, 1987.

[43] H. R. Philipp, "Optical properties of silicon nitride," *Journal of the Electrochemical Society,* vol. 120, pp. 295-300, 1973.

[44] M. Hjelm, B. Norlin, H.-E. Nilsson, C. Fröjdh, and X. Badel, "Monte Carlo simulation of the imaging properties of scintillator-coated X-ray pixel detectors," *Nuclear Instruments and Methods in Physics Research Section A: Accelerators, Spectrometers, Detectors and Associated Equipment,* vol. 509, pp. 76-85, 2003.

[45] S. Mehta, A. Patel, and J. Mehta, "CCD or CMOS Image sensor for photography," in *Communications and Signal Processing (ICCSP), 2015 International Conference on*, 2015, pp. 0291-0294.

[46] W. Boyle and G. Smith, "Three dimensional charge coupled devices," 1974.

[47] S. A. Taylor, "CCD and CMOS imaging array technologies: technology review," *UK: Xerox Research Centre Europe,* 1998.

[48] DALSA Inc. (April 2016). *Advantages and Disadvantages of Various CCD Area Array Sensors* [Application Note]. Available: http://www.teledynedalsa.com/

[49] DALSA Inc., "CCD Technology Primer," in *DALSA Databook*, ed, 1999.

[50] J. T. Bosiers, I. M. Peters, C. Draijer, and A. Theuwissen, "Technical challenges and recent progress in CCD imagers," *Nuclear Instruments and Methods in Physics Research Section A: Accelerators, Spectrometers, Detectors and Associated Equipment,* vol. 565, pp. 148-156, 2006.

[51] F. M. Wanlass, "Low stand-by power complementary field effect circuitry," ed: Google Patents, 1967.

[52] M. Bigas, E. Cabruja, J. Forest, and J. Salvi, "Review of CMOS image sensors," *Microelectronics Journal,* vol. 37, pp. 433-451, 5// 2006.

[53] D. Litwiller, "CMOS vs. CCD: Maturing Technologies, Maturing Markets-The factors determining which type of imager delivers better cost performance are becoming more refined," *Photonics Spectra,* vol. 39, pp. 54-61, 2005.

[54] M. Nikl, "Scintillation detectors for x-rays," *Measurement Science and Technology,* vol. 17, p. R37, 2006.

[55] B. K. Cha, S. J. Lee, P. Muralidharan, J. Y. Kim, D. K. Kim, D. H. Lee*, et al.*, "Synthesis and scintillation properties of nano Gd 2 O 3 (Eu) scintillator for high resolution X-ray imaging applications," *Nuclear Instruments and Methods in Physics Research Section A: Accelerators, Spectrometers, Detectors and Associated Equipment,* vol. 619, pp. 174-176, 2010.

[56] R. Lujan and R. Street, "Flexible X-ray detector array fabricated with oxide thin-film transistors," *IEEE Electron Device Letters,* vol. 33, p. 688, 2012.

[57] M. J. Weber, "Inorganic scintillators: today and tomorrow," *Journal of Luminescence,* vol. 100, pp. 35-45, 2002.

[58] S. V. Ranade, R. E. Richard, and M. N. Helmus, "Styrenic block copolymers for biomaterial and drug delivery applications," *Acta Biomaterialia,* vol. 1, pp. 137-144, 2005.

[59] C. Allier, R. Hollander, C. van Eijk, P. Sarro, M. de Boer, J. Czirr*, et al.*, "Thin photodiodes for a neutron scintillator silicon-well detector," *IEEE Transactions on Nuclear Science,* vol. 48, pp. 1154-1157, 2001.

[60] Z. F. Wang, P. Wang, X. Y. Ye, and B. Jiang, "Processing and modeling of multi-walled carbon nanotube/styrene-butadiene-styrene (SBS) composites for force sensing," in *Nanotechnology, 2009. IEEE-NANO 2009. 9th IEEE Conference on*, 2009, pp. 756-757.

[61] L. Ovechkina, K. Riley, S. Miller, Z. Bell, and V. Nagarkar, "Gadolinium loaded plastic scintillators for high efficiency neutron detection," *Physics Procedia,* vol. 2, pp. 161-170, 2009.

[62] B. Ando and S. Baglio, "Inkjet-printed sensors: a useful approach for low cost, rapid prototyping [Instrumentation Notes]," *IEEE Instrumentation & Measurement Magazine,* vol. 14, pp. 36-40, 2011.

[63] J. Nijs, E. Demesmaeker, J. Szlufcik, J. Poortmans, L. Frisson, K. De Clercq*, et al.*, "Recent improvements in the screenprinting technology and comparison with the buried contact technology by 2D-simulation," *Solar Energy Materials and Solar Cells,* vol. 41, pp. 101-117, 1996/06/01 1996.

[64] R. E. Sousa, C. M. Costa, and S. Lanceros-Méndez, "Advances and future challenges in printed batteries," *ChemSusChem,* vol. 8, pp. 3539-3555, 2015.

[65] S. Pyo, J.-I. Lee, M.-O. Kim, T. Chung, Y. Oh, S.-C. Lim*, et al.*, "Development of a flexible three-axis tactile sensor based on screen-printed carbon nanotube-polymer composite," *Journal of Micromechanics and Microengineering,* vol. 24, p. 075012, 2014.

[66] A. Abdellah, D. Baierl, B. Fabel, P. Lugli, and G. Scarpa, "Exploring spray technology for the fabrication of organic devices based on poly (3-hexylthiophene)," in *Nanotechnology, 2009. IEEE-NANO 2009. 9th IEEE Conference on*, 2009, pp. 831-934.

[67] W. Zhou, A. B. Belay, K. Davis, and N. Sorloaica-Hickman, "Transparent conductive film fabrication by carbon nanotube ink spray coating and ink-jet printing," in *Photovoltaic Specialists Conference (PVSC), 2012 38th IEEE*, 2012, pp. 002324-002327.

[68] Y. Jang, Y. D. Park, J. A. Lim, H. S. Lee, W. H. Lee, and K. Cho, "Patterning the organic electrodes of all-organic thin film transistors with a simple spray printing technique," *Applied physics letters,* vol. 89, p. 183501, 2006.

[69] J. S. Kelly and B. S. Lindblom, *Scientific examination of questioned documents*: CRC press, 2006.

[70] J. Courbat, Y. Kim, D. Briand, and N. De Rooij, "Inkjet printing on paper for the realization of humidity and temperature sensors," in *2011 16th International Solid-State Sensors, Actuators and Microsystems Conference*, 2011, pp. 1356-1359.

[71] X. Liu, T.-J. Tarn, F. Huang, and J. Fan, "Recent advances in inkjet printing synthesis of functional metal oxides," *Particuology,* vol. 19, pp. 1-13, 2015.

[72] Texas Instruments. (June 2016). *TSL235 Light-to-Frequency Converter*. Available: http://www.ti.com

[73] Texas Instruments. (July 2016). *CD405xB CMOS Single 8-Channel Analog Multiplexer/Demultiplexer With Logic-Level Conversion*. Available: http://www.ti.com

[74] Atmel Corporation. (August 2016). *ATmega328P*. Available: http://www.atmel.com/

[75] Arduino. (August 2016). *Arduino/Genuino UNO*. Available: https://www.arduino.cc

[76] Cytec BG. (July 2016). *3D BRD Viewer*. Available: http://3dbrdviewer.cytec.bg/

[77] Arduino. (August 2016). *Arduino Software IDE*. Available: https://www.arduino.cc

[78] Bruker. (August 2016). *D8 Discover*. Available: www.bruker.com

[79] Fujifilm Corporation. (October 2016). *RX EVO-F*. Available: www.fujifilm.eu